Research Square

Preprints are preliminary reports that have not undergone peer review.
They should not be considered conclusive, used to inform clinical practice,
or referenced by the media as validated information.

Extended Cognitive Recovery in Down Syndrome Mice via Sustained Release of Am404 From Microplates

Corinne Portioli
Italian Institute of Technology
Denise Murgia
Italian Institute of Technology
Raffaele Spanò
Italian Institute of Technology
Stefania Mamberti
Italian Institute of Technology
Bianca Martins Estevão
Italian Institute of Technology
Greta Avancini
Italian Institute of Technology
Sine Bertozzi
Italian Institute of Technology
Andrea Armirotti
Italian Institute of Technology
Laura Cancedda
Italian Institute of Technology
Paolo Decuzzi
paolo.decuzzi@iit.it

Italian Institute of Technology

Research Article

Keywords: drug delivery, microparticles, glial cells, anti-inflammatory drugs

Posted Date: August 24th, 2026

DOI: https://doi.org/10.21203/rs.3.rs-10255698/v1

License: This work is licensed under a Creative Commons Attribution 4.0 International License.
Read Full License

Additional Declarations: No competing interests reported.

Abstract

Neurodevelopmental disorders (NDDs) are often characterized by cognitive deficits associated with hippocampal dysfunction and microglial activation. In the in the Dp(16) and Ts65Dn mouse models of Down syndrome (DS), paracetamol (PRC) has been shown to modulate microglia-mediated neuroinflammation and rescue memory tasks. However, the high doses of PRC typically required limit its long-term use due to dose-related toxicity, including reported hepatotoxicity and cardiotoxicity. Here, we employed polymeric microPLates (μPL) made of poly(lactic-co-glycolic acid) (PLGA) to sustain delivery of AM404 (AM404-μPL), the primary PRC metabolite with glia-directed anti-inflammatory activity. Using a top-down fabrication approach, AM404 was loaded into square-shaped μPL and evaluated for activity *in vitro* and *in vivo*. Free AM404 enhanced microglial metabolism and exerted anti-inflammatory effects comparable to paracetamol in activated microglia from Dp(16) mice. *In vivo*, low-dose free AM404 (1 mg/kg for three days) improved cognitive deficits in DS mice without affecting control mice; whereas higher doses (10 mg/kg) impaired cognition in healthy mice and had no effect on DS mice. In contrast, a single injection of AM404-μPL improved DS mice cognition for two weeks without harming healthy mice. Notably, after one week, cognitive abilities in DS mice matched those achieved with repeated low-dose of free AM404. These findings support AM404 sustained delivery as a strategy to maintain therapeutic efficacy while reducing dosing frequency and toxicity, offering a promising approach for treating DS as well as other NDDs.

Introduction

Neurodevelopmental disorders (NDDs) comprise a heterogeneous group of conditions characterized by cognitive, emotional, and motor impairments, often associated with overlapping symptoms and shared dysfunctional pathways [1]. Genetic NDDs, including Down syndrome (DS), Fragile X syndrome, and Rett syndrome, arise from alterations in genes that regulate synaptic function, transcription programs, and epigenetic mechanisms, ultimately affecting neuronal and glial development and function [1, 2]. Among these conditions, DS is the most common genetic cause of intellectual disability and is frequently associated with cognitive impairment, metabolic alterations, and a chronic inflammatory state that may contribute to progressive decline in hippocampal-related functions [3].

Neuroinflammation has emerged as a central and potentially druggable contributor to cognitive dysfunction in DS and other NDDs [4–6]. Microglia, the resident immune cells of the central nervous system, are primary mediators of this response, acting in concert with astrocytes, neurons, oligodendrocytes, and pericytes. While acute neuroinflammatory responses can be protective, persistent microglial activation and sustained production of inflammatory mediators can promote synaptic dysfunction, neuronal damage, and cognitive impairment [4–6]. Incidentally, this also makes DS a valuable model for studying neuroinflammation-related early neurodegenerative processes and the progression toward Alzheimer's disease (AD)-like dementia, which is characteristic of people with DS [7]. In DS, neuroinflammatory alterations arise early in life and are characterized by increased levels of pro-inflammatory cytokines, including IL-1β and TNF-α, as well as microglial hyperactivation, altered glial

morphology, and neuronal loss [8–10]. Unlike the underlying genetic cause of DS, neuroinflammation can be pharmacologically modulated, making it an attractive therapeutic target [11, 12] .

Several therapeutic strategies have been explored to mitigate cognitive impairment in DS, including pharmacological modulation of neuronal excitability, gene-based approaches, and anti-inflammatory interventions [13–15]. Among these, paracetamol (PRC; acetaminophen) has shown the ability to reduce microglia-mediated neuroinflammation and rescue cognitive performance in the Dp(16) mouse model of DS [14, 16]. However, these beneficial effects require repeated, high-dose (100 mg/kg) administration, which may limit long-term applicability because of dose-related toxicity, including hepatotoxicity and possible cardiotoxicity [17–19]. These limitations highlight the need for therapeutic strategies capable of maintaining efficacy, while reducing systemic exposure, dosing frequency, and peak drug concentrations.

AM404, the primary bioactive metabolite of PRC, represents a promising alternative candidate for modulating neuroinflammation. AM404 has been implicated in the central analgesic and anti-inflammatory effects of PRC and has been shown to regulate inflammatory responses in microglial and neuronal models [20–22]. Importantly, AM404 exerts biological activity at substantially lower doses than PRC *in vivo* and has been reported to lack the hepatic toxicity typically associated with high-dose PRC exposure [14, 20–27]. Nevertheless, free small molecules are often limited by rapid clearance, variable tissue exposure, and the need for repeated administration to sustain therapeutic activity. Controlled drug release systems may overcome these limitations by providing prolonged local or systemic drug availability while minimizing repeated dosing and reducing the risk of adverse effects [28].

Poly(lactic-co-glycolic acid) (PLGA)-based microparticles are well-established biodegradable platforms for sustained drug release. Among these, shape-defined polymeric microPLates (μPL) have shown promise as long-acting depots for the controlled delivery of anti-inflammatory and neuroactive compounds [29, 30]. Their geometry, composition, and loading conditions can be engineered to tune fabrication yield, drug loading, degradation, and release kinetics. In this study, we developed AM404-loaded μPL as a sustained-release platform for the treatment of cognitive impairment associated with DS. We optimized square-shaped PLGA μPL for AM404 loading and release, evaluated the effects of AM404 on primary neurons, astrocytes, and microglia, and tested whether free AM404 and AM404-μPL could modulate inflammatory responses and rescue recognition memory deficits in the Dp(16) mouse model of DS. By combining a glia-directed anti-inflammatory metabolite with a long-acting biodegradable delivery system, this work aims to establish a strategy for sustained cognitive benefit while reducing treatment burden and dose-related toxicity.

Results

A top-down fabrication method for AM404 – loaded microPLates. To achieve the sustained delivery of AM404, we fabricated biodegradable polymeric microparticles – microPLates (μPL) – using a multi-step, top-down approach, based on a replica molding technique [29, 30]. To this aim, we first generated a silicon master template, featuring a regular array of equally spaced wells with a 20 · 20 μm square base

and a 10 μm depth, realized by direct laser writing and utilized to define the geometry of μPL (Fig. 1A). We then replicated this master template in a PDMS template as an intermediate step; then, we further replicated it into a PVA template. The PVA template, highly soluble in water, was an exact copy of the original silicon template. Next, we carefully filled the wells in the PVA template with a solution of poly (lactic-co-glycolic acid) (PLGA) dissolved in acetonitrile to form the empty μPL (Empty μPL). Alternatively, we slowly added and dissolved the solid compound AM404 into the polymer solution to form the AM404-loaded μPL (AM404-μPL). We proceeded with vacuum incubation to allow the polymeric solution to enter the wells and dry the thin layer. Finally, we gradually dissolved the PVA template with the loaded wells in a water solution to release the μPL, which we subsequently collected via centrifugation.

To optimize particle yield and drug encapsulation, we fabricated multiple μPL formulations by varying PLGA (5 or 10 mg) and AM404 (375–800 μg) amounts per PVA template. For 5 mg PLGA, we tested all AM404 doses (375, 500, 600, 750, and 800 μg), yielding five μPL configurations. For 10 mg PLGA, we only evaluated the higher AM404 doses (600 and 800 μg). We then characterized all μPL configurations for their morphological properties using scanning electron microscopy (SEM) and a Multisizer Coulter counter system (Figs. 1B **– D**). The SEM images in Fig. 1B display well-defined, square-shaped μPL with an expected edge length of about 20 μm and a height of approximately 10 μm, corresponding to the wells' size in the original silicon master and the PVA sacrificial templates. We observed no significant difference between the Empty μPL and the AM404-μPL size, since the template, rather than the payload, unequivocally determined the particle morphology (**Supporting** Fig. 1). The μPL presented an upward concavity for both PLGA inputs, as if the wells in the PVA template were not fully filled by the polymer solution or the material had compacted during the vacuum step preceding the template's dissolution in water. However, with higher PLGA content, there was a visible increase in the well-filling, which reduced the concavity on top. To further evaluate the μPL morphology across the entire fabrication batch, we used a Multisizer Coulter counter system. Figure 1C provides the size distribution for 5 mg and 10 mg PLGA μPL in aqueous solutions. As anticipated from the SEM analyses, the two profiles overlapped. It is here crucial to note that the Multisizer Coulter counter assumes that the particles are spherical; therefore, the characteristic size associated with the peaks represents an average size of the μPL, including the base edge length of 20 μm and the 10 μm height, returning a typical value of about 17 ± 0.42 μm (5 mg PLGA) and about 19 ± 0.46 μm (10 mg PLGA). From the Multisizer analyses, the number of μPL produced per template could be readily measured and compared to the theoretical number of μPL that could be produced per template (i.e., the number of wells in the original silicon template). The ratio between these two quantities returned the fabrication yield. The bars in Fig. 1D provide the fabrication yield for the 5 mg PLGA μPL, namely Empty (0 μg AM404) and μPL loaded with 375 μg, 500 μg, 600 μg, 750 μg, and 800 μg AM404. We did not find a statistically significant difference among the tested configurations ($p > 0.9$). For the 5 mg PLGA configurations, we recorded the highest fabrication yield for AM404 800 μg with 59 ± 4.5%, followed by AM404 750 μg with 49 ± 4.4%. We calculated comparable fabrication yield values for AM404 600 μg (49 ± 7.6%), AM404 500 μg (55 ± 3.2%), and AM404 375 μg (51 ± 4.2%). The fabrication yield for the 10 mg PLGA μPL was 24 ± 6.1% for AM404 600 μg and 23 ±

4.3% for AM404 800 µg, as documented by the dashed bars in Fig. 1D. When comparing the 5 mg PLGA µPL with the 10 mg PLGA µPL, we observed a statistically significant decrease ($p = 0.0055$) in fabrication yield only for the AM404 800 µg configuration (Fig. 1D, dashed vs empty bars). These findings corroborate the notion that solutions with lower PLGA content (i.e., 5 mg PLGA) are less viscous and can be more efficiently spread on the PVA template and in its wells. This improves spreading into the wells and enhances particle yield per template [29, 30]. This observation was consistent with the peaks observed in the Multisizer spectrum: the lower peak intensity associated with the 10 mg PLGA configuration was related to a lower fabrication yield, possibly caused by challenges in particle formation, which also complicated the purification process (Fig. 1C).

Biodegradation of microPLates under physiological conditions. To assess the morphological changes over time and mimic the prolonged interaction of the µPL with different solutions, we incubated 5 mg and 10 mg PLGA µPL in physiological solution (PBS) or deionized (DI) water at 37°C. We monitored the morphological alterations of µPL over time via SEM and Multisizer Coulter counter analyses, which also tracked any possible reduction in the number of particles. We took SEM images at predetermined time points over an incubation period of 70 days. On day 0, all samples exhibited the characteristic square shape in both PBS and DI water (Figs. 2, **Supporting** Fig. 2 and **Supporting** Fig. 3A). The morphology did not change appreciably for up to 14 days in physiological solution, across all tested configurations. However, we observed clear signs of degradation in the 10 mg samples, mainly for the AM404 600 µg, after just 14 days (**Supporting** Fig. 3A). By day 21, all tested µPL configurations presented early signs of biodegradation, evidenced by a progressive loss of the square shape towards a more rounded morphology, roughening and folding of the side edges. This clearly documented a rearrangement of the shape towards one that would minimize energy for a given volume of material (i.e., sphere) and a loss of mechanical stability (i.e., folding of the edges). We observed a progression in the degradation process at later time points, namely 28, 42, and 70 days. The degradation affected the core of the µPL, transforming them into much smaller globular and flatter polymer assemblies until they became a plethora of small dots by day 70 (Fig. 2).

Given the autocatalytic behavior, µPL biodegradation proceeded more rapidly in DI water than in PBS. Within one week, we observed a quick collapse for all µPL configurations (**Supporting** Fig. 3A). The original morphology was lost in all tested configurations, independent of the PLGA amount used, indicating strong polymer-water interactions. Biodegradation was apparent from the smoothing of the sharp edges and the gradual transition from a square shape to a round morphology. We further validated the biodegradation changes by an increase in particle circularity after one week (**Supporting** Fig. 3B). The hydrolysis of the ester bonds between the lactic acid (LA) and glycolic acid (GA) units in the PLGA chains accelerates in slightly acidic pH (i.e., DI water), which facilitates hydrolysis through hydrogen ions [31]. Conversely, PBS, a buffered ionic solution, stabilizes pH during hydrolysis, thereby slowing PLGA degradation. We also noted large holes inside the structure of the particles, documenting bulk degradation associated with the permeation of water and activation of the autocatalytic process within the particle core.

To help trace modifications over time in μPL size distribution, characteristic size, and number, we used Multisizer Coulter counter analyses (**Supporting** Fig. 4). We found that empty and AM404-loaded μPL gradually changed morphology in physiological conditions (PBS solution), keeping their square shape for 14 days before diminishing over 70 days. In water, strong polymer-water interactions accelerated μPL degradation, leading to a collapse of all μPL configurations after 7 days and a loss of their square shape.

Pharmacological characterization of AM404 – loaded microPLates. We selected as payload the molecule AM404, which is the primary metabolite of PRC, due to its emerging pharmacological effects on immune cells [21, 23]. We characterized all the μPL configurations loaded with AM404 in terms of encapsulation efficiency (EE), defined as the ratio of the mass of AM404 entrapped in the μPL to the total initial mass of AM404 per template (Fig. 3A). Moreover, we measured the amount of AM404-loaded per template (loading μg per template – μg/T), defined as the total mass of AM404-loaded in the μPL per template (Fig. 3B). With respect to the EE, for the 5 mg PLGA μPL configurations, we measured the highest value for the AM404 500 μg, corresponding to 20.0 ± 0.951%, compared to the 15.5 ± 0.909% of the AM404 750 μg and the 16.4 ± 1.00% of the AM404 375 μg (Fig. 3A). In contrast, the AM404 600 μg and 800 μg configurations showed lower EE, corresponding to 10.6 ± 0.612% and 15.3 ± 0.984%, respectively. For the 10 mg PLGA μPL configurations (Fig. 3A), the EE was 14.3 ± 2.56% and 11.1 ± 2.18%, respectively, for the AM404 600 μg and 800 μg. We did not observe significant differences in EE between the 5 mg and 10 mg PLGA μPL configurations for the tested concentrations.

Conversely, we documented significant differences for the loaded amounts of AM404 per template. For the 5 mg PLGA μPL configuration, the loading of AM404 increased significantly with the initial input. Specifically, the total mass of drug loaded per template was 61.6 ± 3.79 μg for the AM404 375 μg, 100 ± 5.69 μg for the AM404 500 μg, and 115 ± 6.77 μg for the AM404 750 μg (Fig. 3B). Moreover, for the 10 mg PLGA μPL configuration, the loading was not significantly affected by the initial input, being 85.8 ± 15.3 μg for the AM404 600 μg and 85.8 ± 15.3 μg for the AM404 800 μg. For the corresponding 5 mg PLGA μPL configuration, the loading values were 122 ± 7.77 μg for the AM404 800 μg and 63.5 ± 3.62 μg for the AM404 600 μg (Fig. 3B). As expected, the loading of AM404 per template decreased as the PLGA content increased due to the more viscous solution and lower fabrication yield of this μPL configuration.

Out of these configurations, we selected three 5 mg PLGA μPL for further investigation regarding the sustained release of the encapsulated molecule. We chose not to use the 10 mg PLGA μPL due to its lower fabrication yield and reduced encapsulation efficiency. We assessed the release kinetics of AM404 from the 5 mg PLGA μPL loaded with 375 μg, 500 μg, and 750 μg under physiological conditions (PBS, pH 7.4, 37°C) over a period of up to 70 days, within a confined volume of 500 μL closely replicating the limited space for intra-tissue depots. We examined the release profiles for the three μPL configurations and presented the percentage of drug released over a 70-day period (Fig. 3C and **Supporting Table 6**). Over the first 28 days of observation, the AM404 375 μg configuration showed a moderately faster release with 49.7 ± 3.63% of the loaded amount being released in 28 days. The AM404 500 μg and 750 μg configurations were associated with slower release rates with 37.6 ± 2.51% and 30.9 ± 4.17% of the drug being released on day 28, respectively. Analyzing the release profile at 70 days, we noted that both

the 375 μg and 500 μg configurations exhibited a similar increase in release kinetics, achieving 77.0 ± 1.06% and 72.5 ± 3.03%, respectively, at the end of the observation period. Differently, the 750 μg configuration reached a plateau of approximately 45.8 ± 0.65% in 70 days. Given the high fabrication yield and loading, and the favorable encapsulation efficiency and release profile, we selected the 5 mg PLGA μPL configuration loaded with 500 μg AM404 for all the following studies.

To address how various configurations differently affected drug release, and to investigate the release mechanisms of AM404, we interpolated data for all configurations considered. Among all the tested kinetic models, the Korsmeyer–Peppas model [32, 33] provided the best fit across all configurations (**Supporting** Figs. 6B and 6C). These data suggest that 5 mg PLGA-500 μg AM404 configuration exhibited significant loading and favourable encapsulation efficiency, along with high fabrication yield and release profile over 70 days. Thus, we chose this configuration for all subsequent *in vivo* studies.

Metabolic effects and cytotoxicity of AM404 on neurons, astrocytes, and microglia. To evaluate the effects of AM404 at increasing concentrations on cell metabolism, we incubated primary cultures of neurons, astrocytes, and microglial cells with free AM404 up to 100 μM. In neurons (Fig. 4A), AM404 slightly reduced the metabolic activity at 0.4, 0.8 and 1.6 μM concentrations, although maintaining a cell metabolism higher than 80%. In fact, we observed signs of toxicity at concentrations higher than 25 μM (cell metabolism ≤ 70%). Conversely, higher doses of AM404 markedly increased metabolism in astrocytes (Fig. 4B). For microglial cells, only AM404 concentrations higher than 25 μM resulted in a significant decrease in metabolism to less than 50% (Fig. 4C).

To specifically assess the efficacy of AM404 in mitigating the inflammatory response, we investigated the effect of AM404 in modulating the lipopolysaccharide (LPS)-induced nitrite production in microglial cells (Fig. 4D). LPS, a component of Gram-negative bacteria's outer membrane, triggers microglial cells to produce inflammatory molecules, primarily nitric oxide (NO) [34]. The Griess assay accurately measures nitrite levels, as they are the stable byproduct of NO. In the same figure, we provided a direct comparison of AM404 with PRC, which served as a benchmark for the FDA-approved anti-inflammatory effect. To evaluate its ability in reducing the inflammatory response in microglial cells, we examined AM404 and PRC using primary cells from a mouse model of DS. We selected the Dp(16) mouse model of DS due to prior observations showing that this model exhibits activated microglial cells, a status that can be reversed by PRC treatment [14]. We also chose Dp(16) mice as they exhibit cognitive impairment as also described in people with DS, since they mimic genetic abnormalities and central nervous system-related alterations [35, 36].

First, we treated primary microglial cells from wild-type (WT) and Dp(16) mice with LPS to induce inflammation, and then we exposed the cells to different concentrations of AM404 and PRC, which did not affect cell metabolism (≤ 20 μM). As expected, the incubation with LPS (+ LPS bar in Fig. 4D) significantly increased nitrite production after 24 hours compared to the untreated cells (-LPS bar). More interestingly, the nitrite concentration increased more in DS-model cells than in WT cells, highlighting the higher sensitivity to inflammatory stimuli. Notably, cells from healthy WT mice did not react to AM404

and PRC, at the considered concentrations. Indeed, we used doses that did not reduce cell metabolism to exclude the possibility that the observed inhibitory effects were due to cytotoxicity. For the Dp(16) cells, after incubation with 2 μM AM404 or 2 μM PRC, nitrite levels remained slightly decreased or unchanged, although not statistically significant. Differently, nitrite levels significantly dropped after incubation with 20 μM of either AM404 or PRC, indicating that both compounds induced a comparable effect in decreasing the inflammatory response.

These results show that free AM404 concentrations exceeding 25 μM are harmful to neurons, boost astrocyte metabolism, and considerably reduce microglial cell metabolism, highlighting a predominantly microglial response. Additionally, these findings demonstrate that AM404 possesses an anti-inflammatory effect akin to that of PRC on LPS-activated microglial cells derived from a mouse model of DS.

Cognitive deficits in mice treated with low and high AM404 doses.

To investigate the *in vivo* anti-inflammatory effects of the PRC metabolite, with the ultimate goal of reducing the drug dosage in chronic treatments and thereby minimizing its peripheral side effects, we first assessed the therapeutic effect of AM404 as a free molecule in healthy wild-type (WT) and Dp(16) mice. We monitored the therapeutic effect through Novel Object Recognition (NOR) test, which assesses long-term memory. We administered AM404 intraperitoneally (i.p.) over three consecutive daily injections, at doses of 1 or 10 mg/kg. Following protocols detailed in the open literature, we used a solution of 10% Tween80, 10% PEG400 and 80% saline as Vehicle (VEH) for the untreated control group. We determined the dosages of AM404 based on prior studies that administered free PRC [14] or free AM404 [25, 37]. At postnatal day 20 (P20), we administered the first injection to the animals, and we exposed them to the 'habituation phase' of the NOR test, where the animal is placed in an empty arena to become familiar to the environment. On postnatal day 21 (P21), we administered the second injection to the same mice, and we exposed them to the 'acquisition phase' of the NOR test, where three objects were introduced in the arena, and the animal was left free to explore them. At postnatal day 22 (P22), we administered the last injection to the mice, and we exposed them to the testing phase of the NOR test, where the animal is placed in the arena and one of the objects explored at P21 is replaced with a new object. We calculated the time spent exploring the new object compared to the familiar ones, which is indicated as Discrimination Index (DI). We used the DI to assess variation in recognizing familiar/novel objects and, therefore, to evaluate learning and memory abilities. We analyzed the video recordings collected during the test phase of NOR test to assess variations in the DI after drug treatment. A schematic representation of the experimental protocol and timing is summarized in Fig. 5A.

At P22, WT mice receiving the higher dose of AM404 (AM404 10 mg/kg) demonstrated a notably lower DI compared to VEH-treated WT mice ($p = 0.0477$), suggesting deficits in behavioral cognitive tasks induced by an excessive dose of the drug. This is in line with previous work showing that treating WT mice with PRC led to a modest decline in cognitive performance on the NOR and Object Location test

(OLT) tests [14]. In contrast, the lower dose of AM404 (AM404 1 mg/kg) showed no significant changes in DI (Fig. 5B), suggesting no toxicity associated with the treatment.

Notably, for Dp(16) mice, the treatment at a lower dose of AM404 improved cognitive impairments, resulting in a statistically higher DI than VEH-treated Dp(16) mice. A higher dose of AM404 did not significantly alter the DI, possibly suggesting again a toxic effect with compromised cognitive activities as observed for the WT mice (Fig. 5D). Of note, weight analysis of the animals, which indicates major toxic effects, revealed no statistically significant differences from the start to the end of the treatment and among the various groups (Fig. 5C, E).

These findings indicate that low doses of AM404 ameliorated cognitive deficits in Dp(16) mice, leading to a statistically increased DI compared to VEH-treated mice, and did not significantly affect the cognitive performance of WT mice, suggesting a lack of treatment toxicity. In contrast, high doses of free AM404 reduced cognitive functions in WT mice while not significantly impacting Dp(16), possibly indicating an optimal tolerated dosage.

Long-lasting cognitive improvement in DS mice with one AM404-μPL administration.

Next, we explored the *in vivo* anti-inflammatory effects of AM404 and its potential to alleviate cognitive impairments, aiming to reduce the frequency of administration to enhance chronic treatment quality. To determine whether a single dose of empty or AM404-μPL could improve cognitive impairment in DS mice without harming WT mice, we first evaluated the anti-inflammatory effects of a single intraperitoneal injection of μPL, at postnatal day 20 (P20), in WT mice. We performed the NOR test at P22, upon a single treatment with Empty or AM404-μPL, to WT mice and subsequently repeated it at P29, P36, and P44. We analyzed the video recordings and determined the DI changes, as shown in Fig. 6A. At all testing time points, the administration of either Empty or AM404-μPL in WT mice did not markedly affect their cognitive functions (Fig. 6B). This suggests that the amount of AM404 released within 44 days after injection was non-toxic and did not lead to changes in cognitive abilities in the WT mice, in contrast to those injected with vehicle or free AM404. We also monitored the weights of WT and DS mice after treatment with AM404-μPL. We found a steady weight gain in the mice over time, consistent with the weight measured for mice treated with empty μPL (Fig. 6C).

Then, we investigated whether the released amount of AM404 was enough to alleviate cognitive decline in DS mice. We evaluated the effect of Empty or AM404-μPL in Dp(16) mice, following the same protocols and timing used for the WT mice, as sketched in Fig. 6A. Upon a single treatment with Empty or AM404-μPL, we performed the NOR test in Dp(16) mice at P22, followed by evaluations at P29, P36, and P44, and we analyzed video recordings to monitor changes in DI (Fig. 7A). At P22, the single administration of AM404-μPL led to a statistically significant improvement in cognitive impairment compared to control Dp(16) mice, which received a single dose of Empty μPL. This finding indicates that AM404 exhibits an anti-inflammatory effect that persisted for up to 48 hours post-injection. Notably, at P22, the cognitive abilities were significantly ameliorated in Dp(16) mice: DI values of mice injected with a single dose of AM404-μPL were comparable to those for Dp(16) mice treated with multiple injections

of free AM404 1 mg/kg (**Supporting** Fig. 7). This suggests that AM404-μPL alleviates cognitive deficits similarly to the free AM404, with one injection of the particles releasing AM404. This achieved comparable efficacy with fewer administrations for three consecutive days. Furthermore, when we re-evaluated the therapeutic effect of AM404-μPL at one-week (P29) or two weeks (P36) post-injection, we found that mice receiving a single dose of AM404-μPL showed marked improvement in cognitive function compared to control Dp(16) mice injected with empty μPL. At P44, we noted an increase in DI of Dp(16) mice, making it unclear whether the released AM404 had an effect or if the mice learned the task during the fourth repetition. Weight changes were monitored to ensure the animal's well-being (Fig. 7B), revealing comparable weights across groups.

These findings suggest that a single μPL injection in WT mice does not harm cognitive functions and indicate that AM404 release post-injection was non-toxic. In DS mice, one injection of AM404-μPL significantly improved cognitive functioning for up to 2 weeks post-injection. At a later time point, DS mice increased the DI, possibly due to retesting, obscuring the effects of released AM404 versus learning in the fourth repetition.

Discussion

Currently, there are no effective treatments for cognitive impairment in DS and its management relies on behavioral lifelong supportive therapies. Given the cognitive impairment and high susceptibility of individuals with DS to early AD and consequent further cognitive decline, there is a critical need for therapeutic strategies targeting cognitive deficits and neuroinflammation. In this context, PRC has been proposed as a candidate therapeutic agent to reduce microglial-mediated neuroinflammation and improve cognitive function [14]. However, despite its widespread clinical use, PRC requires repetitive, high-dose (100 mg/kg) administrations to achieve these effects, raising concerns about hepato- and cardiotoxicity [38, 39]. In this context, several studies identify AM404, the primary lipid metabolite of PRC, as the central mediator of its analgesic and anti-inflammatory effects, with reduced hepatotoxic risk [23, 40]. Its ability to counteract microglia-mediated neuroinflammation is supported by *in vitro* evidence [20–22], and AM404 also exerts neuroprotective effects in primary hippocampal neurons by inhibiting tau toxicity [41]. *In vivo*, AM404 displays anxiolytic, antidepressant-like, and neuroprotective properties across multiple models, including Parkinson's and Alzheimer's disease, and ischemia [26, 41–45]. Chronic low-dose of AM404 (0.25 mg/kg, *i.p.*) improves spatial cognition and reduces pathological features in AD models [41]. However, chronic administration of high doses of AM404 (10 mg/kg) impairs long-term potentiation [46]. Therefore, achieving sustained therapeutic exposure at low doses requires controlled drug delivery systems. Long-acting injectable formulations of AM404 may indeed reduce dosing frequency and improve cognitive outcomes in DS models following a single administration.

In this study, we selected square-shaped microPLates (μPL) as drug-delivery system, due to their proven ability to effectively deliver compounds with physicochemical properties similar to AM404, including antipsychotic agents [47] and anti-inflammatory drugs for osteoarthritis [29]. By varying PLGA and AM404 amounts during fabrication, we identified the 5 mg PLGA – 500 μg AM404 configuration as

optimal due to its significantly higher encapsulation efficiency. This was likely driven by reduced viscosity of the polymeric paste, increased porosity of µPL, resulting in higher fabrication yields and improved drug loading and release profiles. Encapsulation efficiency was comparable to values reported for similar compounds [29, 47]. We also selected the 5 mg configuration to reduce particle size and facilitate *in vivo* administration. Our release studies showed an initial burst followed by sustained AM404 release for up to 70 days, achieved through precise control of µPL geometry and polymer mass. Overall, µPL enabled both immediate drug availability and prolonged release, supporting extended therapeutic exposure.

In parallel, we evaluated free AM404 on primary cell cultures. In neurons and astrocytes, at low concentrations (< 1.6 µM), AM404 slightly reduced metabolic activity while maintaining viability above 80%, whereas higher doses (> 25 µM) induced toxicity and increased astrocytic metabolism. Consistently, AM404 doses up to 0.5 µM were reported as neuroprotective in primary mouse hippocampal neurons [41]. In contrast, studies using the human neuroblastoma cell line SK-N-SH showed no significant viability reduction with AM404 or paracetamol at doses up to 50 µM [20], indicating a possible greater resistance in immortalized cell lines compared to primary neurons and astrocytes. In microglial cells, AM404 concentrations above 25 µM significantly reduced metabolic activity, consistent with prior reports showing no metabolic effects at doses up to 12.5 µM [21, 48]. Given the central role of microglia in NDDs and the well-documented presence of early, persistent neuroinflammation in DS that promotes AD [49] [9, 50], modulating microglial activation represents a promising therapeutic strategy. AM404 has also been proposed to exert neuroprotective effects by modulating oxidative stress and nitric oxide overproduction in Parkinson's disease and neuropathic pain models [42, 51]. *In vitro*, AM404 reduces nitrite formation in BV2 microglial cells at concentrations up to 50 µM [22]. To assess this effect in DS, we exposed primary microglial cells from Dp(16) mice and wild-type (WT) littermates to LPS to induce inflammation and subsequently treated with non-toxic doses of AM404 or PRC (≤ 20 µM). DS-derived microglia showed a greater nitrite response than WT cells, reflecting heightened inflammatory sensitivity. At 20 µM, both AM404 and PRC significantly reduced nitrite levels in primary microglia, whereas only AM404 was effective in BV2 cells, underscoring cell-dependent differences in inflammatory responses [22].

Previous NOR testing showed that chronic paracetamol (PRC, 100 mg/kg) administration for three days rescues cognitive impairments in Dp(16) mice [14]. To evaluate efficacy and toxicity, we administered free AM404 at 1 mg/kg (AM1) or 10 mg/kg (AM10) to WT and DS mice for three consecutive days, and cognitive performance was assessed using the NOR test. AM10 impaired cognition in WT mice and failed to improve performance in DS mice, suggesting dose-related toxicity and behavioral deficits. In contrast, AM1 had no adverse effects in WT mice and significantly improved cognitive impairments in DS mice. These findings highlight dosage as a critical factor, consistent with prior reports showing beneficial effects of low-dose AM404 in AD models [41], while high doses impair long-term potentiation [46]. Accordingly, sustained drug delivery via polymeric microparticles may enable prolonged low-dose administration while minimizing cognitive side effects in WT mice.

Single injections of either empty or AM404-μPL did not affect cognitive function in WT mice, indicating good tolerability and particle inertness. In DS mice, a single AM404-μPL administration significantly improved cognitive deficits compared to empty μPL controls and produced effects comparable to repeated low-dose free AM404, indicating preserved drug activity. Cognitive improvement was evident for up to two weeks and diminished by the third week, possibly due to task learning in control mice rather than reduced treatment efficacy. WT and DS mice treated with free AM404 showed normal weight gain consistent with physiological growth rates (~ 1 g/day at this age [52]), suggesting the absence of systemic toxicity. Similarly, weight changes following AM404-μPL treatment mirrored those of empty μPL controls, confirming particle biocompatibility, in line with prior studies using risperidone-loaded μPL [47]. These findings indicate that a single AM404-μPL injection can sustain cognitive benefits for several weeks without detectable side effects. Prolonged therapeutic efficacy is likely driven by the controlled release of AM404 from μPL, maintaining effective drug exposure while reducing dosing frequency. However, later time points showed ambiguous outcomes, potentially due to task retesting effects or age-dependent glial changes that may not directly translate into cognitive improvement, as previously reported [14]. Additional long-term assessments are needed to disentangle drug-specific effects from learning-related adaptations and to define the true duration of AM404-μPL efficacy.

Conclusion

We designed square-shaped microscopic polymeric particles (microPLates – μPL) as a sustained-release system for AM404, the principal metabolite of PRC, chosen for its promising role in modulating neuroinflammation and improving cognitive function in brain disorders. Following a single administration of AM404-loaded μPL (AM404-μPL) in DS mice, the treatment significantly improved object recognition abilities, without adverse effects on healthy wild-type mice. These findings suggest that AM404-μPL could act as a long-lasting depot system, delivering therapeutic effects over an extended period from a single administration. Looking ahead, future studies will focus on refining μPL fabrication methods to enhance drug loading and encapsulation efficiency, aiming to minimize polymer volume, while increasing drug concentration and improving safety. This approach not only strengthens the therapeutic potential of the current system but also opens new avenues for adapting the platform to other bioactive compounds and brain disease models. Embracing a more integrated and stratified research pipeline will be crucial for developing effective, targeted treatments for cognitive alterations across a broader range of neurological disorders.

Materials and methods

Reagents and Materials. Polydimethylsiloxane (PDMS, Sylgard 184) and elastomer were purchased from Dow Corning Corp (Midland, US). Poly(vinyl alcohol) (PVA, Sigma-Aldrich Mw 9000 – 10000), poly(D,L-lactide-co-glycolide) acid (PLGA, Sigma-Aldrich Resomer® RG504 H lactide:glycolide 50:50, Mw 38,000 – 54,000), sucrose (Sigma-Aldrich, product code S7903), bovine thrombin (Sigma-Aldrich, product code 605157), deoxyribonuclease I from bovine pancreas (DNAse) (Sigma-Aldrich, product code D5025-150KU), thiazolyl Blue tetrazolium bromide, 98% (Sigma-Aldrich, product code M2128-1G), Triton™ X-100

(Sigma-Aldrich X100), poly-D-Lysine hydrobromide (PDL) (Merck Life Science, product code P6407-5MG) and bovine serum albumin (BSA) (product code A9418) were purchased from Merck (Merck KGaA, Darmstadt, DE). N-arachidonoylphenolamine (AM-404) (product code 10-2008-50mg) was purchased from DBA Italia (Segrate, Milan), deuterated AM404 (AM404-d4) (product code sc-217618) was purchased from Santa Cruz Biotechnology, Inc. (Dallas, US). Paracetamol (Acetaminophen) (Sigma-Aldrich, product code P0300000 50mg). ClearLine® sterile cell strainer 40 µm was from dDBioLab (Dutscher group, ES). Hanks' balanced salt solution (HBSS) (product code 14175095), trypsin 0.25% phenol red (product code 25050014), trypsin-EDTA (0.25%) phenol red (product code 25200056), DMEM/F-12 (Dulbecco's Modified Eagle Medium/Nutrient Mixture F-12), GlutaMAX™ supplement (product code 31331028), heat inactivated (HI) Horse Serum (HS) (26050088), penicillin-streptomycin PEN-STREP (10,000 U/mL) solution (product code 15140122), Trypan Blue Solution 0.4% (product code 15250061) and Dulbecco's phosphate-buffered saline (DPBS), no calcium, no magnesium (product code 14190144) were purchased from Gibco FisherScientific (ThermoFisher Scientific, Waltham, MA, US). Multisizer 4e Coulter Counter, Accuvette ST Sampling Vials (product code A35471), and ISOTON® II Diluent were from Beckman Coulter (Cassina De' Pecchi, Milan, IT). GraphPad Prism was from GraphPad Software (San Diego, California, US). All schematics were created with BioRender Software.

Fabrication of AM404-loaded and empty microPLates (µPL). AM404-loaded µPL (AM404-µPL) and empty µPL were synthesized using a multistep top-down approach, described previously from our group [29, 53–55] and refined in a recent work [30]. In the fabrication process, direct laser writing technique was employed to obtain the silicon master template with arrays of square-shaped wells to obtain µPL with a defined geometry of 20x20 µm (in edge length) and 10 µm (in depth), separated by a gap of 5 µm. The silicon template was replicated by covering it with a mixture of PDMS and drug (10:1, v/v), followed by a step in a vacuum chamber to remove the bubbles and a step in the oven at ~ 60°C for 8 hours to favor polymerization. Then, the PDMS template was carefully peeled off the silicon master and used to obtain sacrificial PVA templates. The PVA templates were obtained by pouring a PVA solution (5% w/v in deionized (DI) water) on the PDMS patterned surface. The sample was then dried at ~ 60°C to obtain a PVA film that was finally peeled off the PDMS template, presenting the same array of wells as the original silicon master mold. In the last fabrication step, the wells of the PVA template were filled by carefully spreading the polymeric paste with the help of a pipette tip. For each PVA template, the paste was obtained by dissolving in ACN different amounts of polymer (5 mg or 10 mg) and various amounts of AM404 (375 µg, 500 µg, 600 µg, 750 µg, and 800 µg). The solvent evaporation was then controlled by leaving the samples in a vacuum chamber for 10 min. Then, the loaded PVA templates were dissolved in DI water at room temperature in an ultrasonic bath. The following purification step was carried out by filtering the DI solution containing the dissolved PVA templates, through polycarbonate membrane filters (40 µm pore size) to remove residual pieces of PVA. Purified µPL were recovered after two sequential centrifugation steps (5,000 rpm for 5 min) and stored at 4°C as a wet pellet, for further use. Empty µPL were fabricated following the same sequential process, with the PVA template loaded with a solution containing only polymer. Within this process the different empty and loaded µPL configurations were fabricated and characterized.

Morphological and dimensional characterization of microPLates (μPL). μPL were characterized for yielding and geometry after purification using different techniques. The μPL number per PVA template and the size distribution were calculated using a Multisizer 4E Coulter Particle Counter (Beckman Coulter, CA). For the analysis, 10 μL of each μPL configuration suspension was transferred to a Multisizer Cuvette with 20 mL of ISOTON® II Diluent (Beckman Coulter). The measurements were run in technical triplicates, using a 100 μm aperture Multisizer capillary. The fabrication yield percentage (Yield %) was calculated using the following formula: (experimental number of particles / theoretical number of particles) x 100, where the theoretical number of particles was calculated based on the template design (486,903 particles/ template). μPL geometry was confirmed using scanning electron microscopy (SEM, Helios Nanolab 650, FE). For SEM imaging, a sample drop of each configuration was spotted on a glass template and uniformly sputtered with 10 nm of carbon to increase the contrast and reduce sample damage. SEM image acquisition was done using an acceleration voltage of 10 keV.

Physico-chemical characterization of microPLates (μPL). The degradation of μPL was evaluated *in vitro* via SEM and Multisizer counter analysis, over time. Briefly, AM404-loaded and empty μPL were incubated in 500 μL of DI water or PBS, under mild mechanical stirring at 37°C. At different time points (0 day, 7 days, 14 days, 21 days, 28 days, 42 days, 70 days), samples were analyzed to assess morphological and structural changes.

Pharmaceutical characterization of microPLates (μPL). The AM404 encapsulation efficiency percentage (EE%) and the AM404 amount per μPL were quantified. Briefly, AM404 EE into AM404 loaded-μPL were evaluated by lyophilizing the μPL and dissolving them in ACN/DI water (1:1, v/v). The samples were then analyzed by high-performance liquid chromatography (HPLC) (Agilent 1260 Infinity, Germany), equipped with a 100 μL sample loop injector and a C18 column (2.1 × 100 mm, 3.5 μm particle size, Agilent Eclipse Plus, USA) for chromatographic separation. For AM404 elution, the mobile phase consisted of DI water with TFA (0.1% v/v) and ACN with TFA (0.1% v/v) pumped in gradient flow rate of 0.3 mL/min from 0 to 17 min, starting at the ratio of 50:50 (v/v), followed by 70%, 80%, and 100% of ACN in 2 min, 4 min and 10 min to lower to 50% in 2 min and maintaining the isocratic ratio of 50:50 (v/v) for 5 min. The signal was detected at a wavelength of 250 nm and the amount of AM404 was interpolated using a standard calibration curve in ACN/DI water (1:1, v/v) in the linear range of 0.2 – 200 μg/mL. No interferences were observed among AM404, PLGA and other components of the measured solution at the testing concentrations. No change in the drug elution peak was observed. EE%, and AM404 amount per μPL were defined using the following formula: (mass of AM404 loaded/mass AM404 input) x 100 and (mass of AM404 loaded/number of μPL) x 100, respectively. To study AM404 release, AM404-μPL and empty μPL, as control, were incubated in 500 μL PBS under mechanical stirring at 37°C. At fixed time points (0 day, 1 day, 7 days, 14 days, 21 days, 28 days, 35 days, 56 days, 70 days), to quantify the amount of AM404 released, the samples in triplicate were collected and centrifuged (12000 rpm for 5 min), discharging the supernatants. Pellets were dissolved in ACN/DI water (1:1, v/v) and analyzed by HPLC using the abovementioned method. The experimental release data were elaborated by GraphPad Prism 10 (GraphPad Software, San Diego, CA, USA) and fitted to different models describing drug release

kinetics. To interpret the AM404 release profile, the experimental data were fitted to the Korsmeyer–Peppas model equation.

Primary glial cells isolation. Glial cell cultures were prepared from C57BL/6J mice at P1 – P2. After the pups were sacrificed by dislocation, all the steps were performed in Petri dishes with ice-cold HBSS and sitting on ice. The skull and cerebral dura mater were removed, and brains were extracted from the skull and transferred into a new dish. Meninges were pulled out, and cortices were dissected from the brain and placed in cold HBSS. 3–4 brains were moved into a 15 mL sterile tube containing 3–4 mL of 0.25% trypsin in HBSS, and 500 µL of DNAse I stock. Deoxyribonuclease I from bovine pancreas was prepared at 25 mg/mL in HBSS and stored at -20°C. The tissue was incubated in water bath at 37°C for 15 min, and mixed gently turning the tube every 5 min. At the end of the process, 10 mL of complete glial cells media (DMEM/F12-GlutaMAX, 10% HS and 1% of PS solution) was added to stop the digestion. The cells were centrifuged for 5 min at 270 g, the supernatant was carefully removed, and 3–4 mL of fresh glial cell media was added. The tissue was then dissociated into a single cell suspension pipetting 10 times. The dissociated cells were passed through a 40 µm strainer, placed onto a 50 mL centrifuge tube, to filter out any remaining tissue fragments. Live cells were counted in a hemacytometer by mixing 10 µL of cell suspension with 10 µL of 0.4% Trypan blue, then the appropriate volume of glial cell media was added to get the desired cell density.

Microglial primary cells isolation using the shaking method. Microglial cells were selected using the shaking method (Giulian and Baker, 1986). Cells extracted were plated on PDL coated 75 cm^2 culture flasks and grown at 37°C in 5% CO_2 incubator in glial cell media. Cells were grown at 37°C in 5% CO_2 humidified atmosphere. After 1 day, the total volume of media was refreshed and exchanged with fresh media, to remove debris and unattached cells, and afterward every 4–5 days, half of the volume was exchanged with fresh media maintained in culture for 14 days (DIV14). At DIV14, pure microglial cells were obtained by shaking the flasks for 3 hours at 250 rpm and 37°C. Floating cells were removed, pelleted at 270 rcf for 5 minutes, and counted. Microglial cells were sub-cultured at $6{\cdot}10^4$ cells/well in 96-well plates with mixed glia-conditioned medium and used after 2 days for cell metabolic activity.

Microglial primary cells isolation using mild trypsinization. Microglial cell cultures were prepared from pups of the same litters: C57BL/6J mice (wild type, WT) and Dp(16) mice, at P1-P2 and kept separated during all isolation. Following the steps describe above to isolate mixed glial cells, in the last step the cells were plated on PDL (0.1 mg/mL) coated 24-well plates at a density of 10 – $12{\cdot}10^4$ cells/well in 500 µL of media. Glial medium was replaced every 4–5 days and confluency was reached at DIV14. At DIV 21 the mild trypsinization method, was used to isolate pure microglial cells, detaching the upper layer of astrocytes in a compact sheet of cells, while microglial cells stay on the bottom of the well [56]. Cells were treated with 0.25% Trypsin, 1 mM EDTA in HBSS, diluted 1:4 in DMEM/F12-GlutaMAX for 40 minutes at 37°C in 5% CO_2 incubator. After that, the media were replaced with complete glia media and cells were left at 37°C in 5% CO_2 incubator for 2 days before using them.

Astrocyte primary cells isolation. Following the shaking step needed to isolate microglial cells, the 75 cm^2 culture flasks were rinsed twice with DPBS, and 5 mL of 0.25% Trypsin-EDTA was added. The flasks were placed in the incubator at 37°C and after 30 min, the cells detachment was enforced by hitting the flask bottom with the hand for a few times. 5 mL of complete glial cell media were added to block trypsin activity and collect the cells. The media containing cells was centrifuged at 270 rcf for 5 min, and the supernatant removed. The pelleted cells were resuspended in fresh pre-heated media and living cells were counted and seeded to have a cell density of 6 x 10^4 cells/well in 96-well plate. Cells were maintained at 37°C in 5% CO_2 incubator for 2 days, then cells were treated for 24 hours with different concentrations of free AM404 and viability assay was performed.

Primary cortical neurons isolation. Pregnant rats were ordered by Charles River Laboratories (Italy). Upon sacrifice of the pregnant rat, the placenta was immediately placed in Hanks' balanced salt solution (HBSS). At embryonic day 17 (E17), embryos were detached and decapitated with scissors, brains displaced from the skulls with surgical tweezers and placed in cold HBSS. After dividing the two hemispheres, the meninges, the corpus striatum, and the hippocampus were discarded to obtain the cortices. The dissected tissue was then incubated for 30–45 minutes in a digestion solution (0.125% Trypsin, 25 µg DNase in 5 mM $CaCl_2$/HBSS per mL of medium per cortex). Neurobasal medium (NB) supplemented with 1% penicillin/streptomycin, 1% GlutaMAX, 2% B-27) with 10% heat-inactivated horse serum (HS) was added to inactivate trypsin prior to 5 min centrifugation at 1,200 rpm. Discarded supernatant, fresh 10% HS NB was added before dissociating tissue through gentle pipetting 10 times. Upon filtering through a 40 µm cell strainer, cells were centrifuged again for 7 min at 700 rpm, counted, and resuspended in complete NB before plating at $3{\cdot}10^4$ cells/well in 0.01% PDL-coated 96-wells plates. Every 3–4 days, 50% of cell culture media were replaced with fresh supplemented NB. Cells were maintained at 37°C in 5% CO_2 incubator for 7 days, then used to perform metabolism assays.

Cell metabolic activity assay. An MTT assay is a colorimetric assay that detects the color change from yellow of the thiazolyl blue tetrazolium bromide dye to purple due to the formation of formazan in the presence of viable cells with active metabolism. Purified microglial cells, astrocytes, and cortical neurons were cultured in 96-well plates as described above, and maintained at 37°C in 5% CO_2, in DMEM/F-12, GlutaMAX medium supplemented with 10% HS, 1% PS. Cells were treated for 24 hours with media only as control and different concentrations of AM404 (0.4 µM, 0.8 µM, 1.6 µM, 3.1 µM, 6.3 µM, 12.5 µM, 25 µM, 50 µM, 100 µM). At the end of the designated incubation times, culture media were replaced with MTT solution in DMEM (5 mg/mL), and cells were incubated for 4 hours at 37°C to allow for cellular metabolism of the tetrazolium dye. MTT was removed and replaced with absolute ethanol (200 µL/well) to lyse the cells and solubilize the formazan crystals. We quantified cell metabolism, evaluating the intensity of the color change in thiazolyl blue tetrazolium bromide dye, which occurs due to formazan production by viable, metabolically active cell metabolism. The intensity of the dissolved product was quantified using a spectrophotometer at 570 nm, with 650 nm as the reference wavelength (Tecan Spark, Tecan Group Ltd., Switzerland). The percentage of cell metabolism was assessed according to the following equation: $(Abs_t/Abs_c){\cdot}100$, where Abs_t and Abs_c are the absorbance of treated

cells and untreated (control) cells, respectively. A decrease in cell viability exceeding 30% is classified as cytotoxic, as per the ISO 10993-5:2009 protocol's guidelines [57].

Griess assay to detect nitrite production. Nitric oxide released by primary WT and Dp(16) microglial cell cultures was quantified indirectly by measuring the accumulation of nitrites (NO_2) as the stable breakdown product of NO and molecular oxygen. Pure microglial cells obtained using the trypsinization protocol described above, were treated with AM404 (AM) or paracetamol (PRC) or DMSO 0.1% (control) for 30 minutes, then LPS (100 ng/mL) was added to each well and left at 37°C in 5% CO_2 incubator for 24 hours. Then, 50 µL of cell culture conditioned supernatant from each well of a 24-well plate were transferred to a 96-well plate. An equal volume of Griess reagent, prepared immediately by combining 1% sulfanilamide, 0.1% N-(1-naphthyl) ethylenediamine dihydrochloride, and 2.5% phosphoric acid was then added to each well and absorbance was measured at 540 nm. Absorbance values for test wells were normalized relatively to control supernatants obtained from unstimulated cells and nitrite concentration was calculated from the standard curve obtained by using sodium nitrite solutions at different concentrations.

Animals. All care of animals and experimental procedures were approved by the Italian Ministry of Health and were conducted in accordance with the Guide for the Care and Use of Laboratory Animals of the National Institute of Health and the European Community Council Directives. All animal procedures were performed following the Italian laws and under the approval by the IIT ethical committee for animal experiments and the Italian Ministry of Health. All animals were housed in a climate-controlled animal facility (22 ± 2°C) and maintained on a 12-hour light/dark cycle with ad libitum access to food and water. Animal housing rooms are maintained at MP14 barrier (pathogen and opportunistic free) in the animal facility before experiments. The Dp(16)1Yey/+ animals were purchased from The Jackson Laboratory (B6.129S7-Dp(16Lipi-Zbtb21)1Yey/J, catalog #013530) and were used to create a colony by mating Dp(16) males with C57BL6/J females. In this study, both male and female mice were used for all experiments.

AM404 andin vivotherapeutic treatments. AM404 powder was dissolved in the vehicle solution. A 2 mg/mL stock solution was prepared in vehicle solution (10% Tween80, 10% PEG400 and 80% saline). The powder was weighed and slowly dissolved first in the corresponding volume of Tween 80, followed by a slight sonication. Then PEG400 and saline were added and the solution kept at 4°C until use. We administered through an intraperitoneal (*i.p.*) injection of 5 mL/kg, a dose of 1 mg/kg or 10 mg/kg of AM404 per mouse [25, 37]. Animals were treated with AM404 or vehicle once daily for three consecutive days, from P20 to P22, 30 minutes before the behavioral test. Mice treated with AM404 loaded-µPL received a single injection at postnatal day 20 (P20). The amount of injected µPL contained the amount of AM404 (µPL containing 100 µg for a 10 g mouse), 10 mg/kg, was equal to the total administered once daily, and in line with the release kinetics. The corresponding amount of µPL was resuspended in saline solution, and 10 mL/kg of particle suspension was *i.p.* injected. Animals were treated with either loaded or empty µPL (corresponding average number of µPL per experiment) as controls and behavioral analyses were carried out at defined time points. To decrease the number of utilized animals in

agreement with ethical guidelines from the Italian Ministry of Health, all vehicle-treated animals from all experiments from P20 to P22 were pooled together. For every acetaminophen-treated litter, at least one animal of each strain was treated with vehicle (except for cases where the number of animals in a given litter did not allow for such precaution no controls were assigned to the litter).

Behavioral experiments. Animals were group-housed (3–5 per cage) based on the littermates and kept at constant room temperature (22 ± 2°C) and relative humidity (60%), with a 12-hour light/dark cycle (7 am – 7 pm). Animals had free access to food and water. Distinct cohort of animals were used for each experiment. Mice were handled 2–3 days before the start of the treatment. All experiments were carried out during the light phase. At least 1 hour prior to the beginning of the test, animals were allowed to acclimatize to the testing room. Behavioral experiments were performed on both male and female mice in the dark. Different litters of animals were used for the novel object recognition (NOR) tests. The NOR was performed as previously described [58] along three days, using a gray acrylic open-field square arena (44 · 44 · 44 cm, Ugo Basile, Gemonio, Italy). Briefly on day 1, the mice were allowed to habituate to the apparatus by freely exploring the open arena for 15 min. On day 2, during the acquisition sessions, three objects different in shape, color, size and material were placed into the arena, and the mice were allowed to explore for 15 min. All sessions of the tests were recorded using a camera (Sony videocam PJ330E). The time spent exploring each object was scored from the recorded videos, with the automatic Anymaze software. The object exploration and preference were evaluated during these sessions to rule out any eventual intrinsic bias. 24 hours later, on day 3, the testing occurred in the same arena. One of the objects used in the acquisition session was replaced by a novel object, and the mice were allowed to explore freely for 15 minutes. The objects were counterbalanced between the sessions, and objects and arena were cleaned with 70% ethanol after each trial, to avoid olfactory cues. The exploratory behavior toward an object was defined as direct contact with the object by the animal's mouth, nose or paws or as an instance when the animal approached the object so that its nose was within 1.5 cm of the object. Any indirect or accidental contact with the objects was not included in the scoring. The time spent exploring each object, expressed as a percentage of the total exploration time, was measured for each trial using an automatic analysis (Anymaze software). The discrimination index was calculated as the difference between the percentage of time spent investigating the novel object and that of time spent investigating the familiar objects: Discrimination Index = ((Novel Object Exploration Time/Total Exploration Time) x 100) - ((Familiar Object Exploration Time/Total Exploration Time) x 100. For the experiments at different time points (P20-P22, P27-P29, P34-P36, P42-P44) on the same groups of animals, completely different sets of objects were used.

Statistical analysis. The GraphPad Prism 10 software (GraphPad Software, USA) was used for statistical analysis. The statistical analysis was performed by unpaired t-test (comparisons between two groups), one-way analysis of variance (ANOVA) followed by Šídák's post hoc test (comparisons among three or more groups).

Declarations

Acknowledgements

This work was partially supported by the EU's Horizon 2020 Research and Innovation Programme under the MSCA grant agreement no. 754490 (COFUND 2018 MINDED), and the Fondazione Istituto Italiano di Tecnologia – IIT. We are grateful to Marina Nanni for training and support in the dissection and isolation of glial cells, to Monica Morini, Antonella Brizzolara, Sara Morando, Daniela Cantatore, Federica Piccardi, and all the animal Facility staff for their precious support and needful advice.

Clinical Trial

Clinical trial number: not applicable.

References

1. Parenti I, Rabaneda LG, Schoen H, Novarino G. Neurodevelopmental Disorders: From Genetics to Functional Pathways. Trends Neurosci. 2020;43:608–21. https://doi.org/10.1016/j.tins.2020.05.004.
2. Zoghbi HY, Bear MF. Synaptic dysfunction in neurodevelopmental disorders associated with autism and intellectual disabilities. Cold Spring Harb Perspect Biol. 2012;4:a009886. https://doi.org/10.1101/cshperspect.a009886.
3. Lorenzon N, Musoles-Lleó J, Turrisi F, Gomis-González M, De La Torre R, Dierssen M. State-of-the-art therapy for Down syndrome. Dev Med Child Neurol. 2023;65:870–84. https://doi.org/10.1111/dmcn.15517.
4. Ahmed MM, Johnson NR, Boyd TD, Coughlan C, Chial HJ, Potter H. Innate Immune System Activation and Neuroinflammation in Down Syndrome and Neurodegeneration: Therapeutic Targets or Partners? Front Aging Neurosci. 2021;13:718426. https://doi.org/10.3389/fnagi.2021.718426.
5. Thomas SD, Abdalla S, Eissa N, Akour A, Jha NK, Ojha S, Sadek B. Targeting Microglia in Neuroinflammation: H3 Receptor Antagonists as a Novel Therapeutic Approach for Alzheimer's Disease, Parkinson's Disease, and Autism Spectrum Disorder. Pharmaceuticals. 2024;17:831. https://doi.org/10.3390/ph17070831.
6. Bartesaghi R, Haydar TF, Delabar JM, Dierssen M, Martínez-Cué C, Bianchi DW. New Perspectives for the Rescue of Cognitive Disability in Down Syndrome. J Neurosci. 2015;35:13843–52. https://doi.org/10.1523/JNEUROSCI.2775-15.2015.
7. Lott IT, Head E. Dementia in Down syndrome: unique insights for Alzheimer disease research. Nat Rev Neurol. 2019;15:135–47. https://doi.org/10.1038/s41582-018-0132-6.
8. Silva MN, Lula MD, Felício LR, Santos B, Nassif LS, Borin MC, Alvares-Teodoro J, Acurcio FDA. Guerra Júnior, Genetic markers involved in neuroinflammation in Down syndrome: a systematic review. Dement Neuropsychol. 2025;19:e20240251. https://doi.org/10.1590/1980-5764-dn-2024-0251.
9. Flores-Aguilar L, Iulita MF, Kovecses O, Torres MD, Levi SM, Zhang Y, Askenazi M, Wisniewski T, Busciglio J, Cuello AC. Evolution of neuroinflammation across the lifespan of individuals with Down syndrome. Brain J Neurol. 2020;143:3653–71. https://doi.org/10.1093/brain/awaa326.

10. Huggard D, Kelly L, Ryan E, McGrane F, Lagan N, Roche E, Balfe J, Leahy TR, Franklin O, Doherty DG, Molloy EJ. Increased systemic inflammation in children with Down syndrome. Cytokine. 2020;127:154938. https://doi.org/10.1016/j.cyto.2019.154938.
11. Zhang W, Xiao D, Mao Q, Xia H. Role of neuroinflammation in neurodegeneration development, Signal Transduct. Target Ther. 2023;8:267. https://doi.org/10.1038/s41392-023-01486-5.
12. Kip E, Parr-Brownlie LC. Healthy lifestyles and wellbeing reduce neuroinflammation and prevent neurodegenerative and psychiatric disorders. Front Neurosci. 2023;17:1092537. https://doi.org/10.3389/fnins.2023.1092537.
13. De Lagran MM, Elizalde-Torrent A, Paredes R, Clotet B, Dierssen M. Lamivudine, a reverse transcriptase inhibitor, rescues cognitive deficits in a mouse model of down syndrome. J Cell Mol Med. 2022;26:4210–5. https://doi.org/10.1111/jcmm.17411.
14. Pinto B, Morelli G, Rastogi M, Savardi A, Fumagalli A, Petretto A, Bartolucci M, Varea E, Catelani T, Contestabile A, Perlini LE, Cancedda L. Rescuing Over-activated Microglia Restores Cognitive Performance in Juvenile Animals of the Dp(16) Mouse Model of Down Syndrome. Neuron. 2020;108:887–e90412. https://doi.org/10.1016/j.neuron.2020.09.010.
15. Parrini M, Naskar S, Alberti M, Colombi I, Morelli G, Rocchi A, Nanni M, Piccardi F, Charles S, Ronzitti G, Mingozzi F, Contestabile A, Cancedda L. Restoring neuronal chloride homeostasis with anti-NKCC1 gene therapy rescues cognitive deficits in a mouse model of Down syndrome. Mol Ther J Am Soc Gene Ther. 2021;29:3072–92. https://doi.org/10.1016/j.ymthe.2021.05.023.
16. Zhang X-W, Feng N, Liu Y-C, Guo Q, Wang J-K, Bai Y-Z, Ye X-M, Yang Z, Yang H, Liu Y, Yang M-M, Wang Y-H, Shi X-M, Liu D, Tu P-F, Zeng K-W. Neuroinflammation inhibition by small-molecule targeting USP7 noncatalytic domain for neurodegenerative disease therapy. Sci Adv. 2022;8:eabo0789. https://doi.org/10.1126/sciadv.abo0789.
17. Baryakova TH, Pogostin BH, Langer R, McHugh KJ. Overcoming barriers to patient adherence: the case for developing innovative drug delivery systems. Nat Rev Drug Discov. 2023;22:387–409. https://doi.org/10.1038/s41573-023-00670-0.
18. Liao X, Li L, Tian J, Chen Z. The relationship between parental stress and treatment adherence in parents of children with neurodevelopmental disorders: A cross-sectional study. Res Dev Disabil. 2025;158:104941. https://doi.org/10.1016/j.ridd.2025.104941.
19. Thai PN, Ren L, Xu W, Overton J, Timofeyev V, Nader CE, Haddad M, Yang J, Gomes AV, Hammock BD, Chiamvimonvat N, Sirish P. Chronic Diclofenac Exposure Increases Mitochondrial Oxidative Stress, Inflammatory Mediators, and Cardiac Dysfunction, Cardiovasc. Drugs Ther. 2023;37:25–37. https://doi.org/10.1007/s10557-021-07253-4.
20. Apweiler M, Streyczek J, Saliba SW, Ditrich J, Muñoz E, Fiebich BL. Anti-Inflammatory and Anti-Oxidative Effects of AM404 in IL-1β-Stimulated SK-N-SH Neuroblastoma Cells. Front Pharmacol. 2021;12:789074. https://doi.org/10.3389/fphar.2021.789074.
21. Saliba SW, Marcotegui AR, Fortwängler E, Ditrich J, Perazzo JC, Muñoz E, De Oliveira ACP, Fiebich BL. AM404, paracetamol metabolite, prevents prostaglandin synthesis in activated microglia by

inhibiting COX activity. J Neuroinflammation. 2017;14:246. https://doi.org/10.1186/s12974-017-1014-3.

22. Slattery WT, Klegeris A. Acetaminophen metabolites p-aminophenol and AM404 inhibit microglial activation. Neuroimmunol Neuroinflammation. 2018;5:11. https://doi.org/10.20517/2347-8659.2018.05.
23. Mallet C, Desmeules J, Pegahi R, Eschalier A. An Updated Review on the Metabolite (AM404)-Mediated Central Mechanism of Action of Paracetamol (Acetaminophen): Experimental Evidence and Potential Clinical Impact. J Pain Res Volume. 2023;16:1081–94. https://doi.org/10.2147/JPR.S393809.
24. La Rana G, Russo R, Campolongo P, Bortolato M, Mangieri RA, Cuomo V, Iacono A, Raso GM, Meli R, Piomelli D, Calignano A. Modulation of Neuropathic and Inflammatory Pain by the Endocannabinoid Transport Inhibitor AM404 [N-(4-Hydroxyphenyl)-eicosa-5,8,11,14-tetraenamide]. J Pharmacol Exp Ther. 2006;317:1365–71. https://doi.org/10.1124/jpet.105.100792.
25. Campolongo P, Ratano P, Manduca A, Scattoni ML, Palmery M, Trezza V, Cuomo V. The endocannabinoid transport inhibitor AM404 differentially modulates recognition memory in rats depending on environmental aversiveness. Front Behav Neurosci. 2012;6. https://doi.org/10.3389/fnbeh.2012.00011.
26. Bortolato M, Campolongo P, Mangieri RA, Scattoni ML, Frau R, Trezza V, La Rana G, Russo R, Calignano A, Gessa GL, Cuomo V, Piomelli D. Anxiolytic-Like Properties of the Anandamide Transport Inhibitor AM404, Neuropsychopharmacology 31 (2006) 2652–9. https://doi.org/10.1038/sj.npp.1301061
27. Bazan HA, Bhattacharjee S, Reid MM, Jun B, Polk C, Strain M, St Pierre LA, Desai N, Daly PW, Cucinello-Ragland JA, Edwards S, Recio J, Alvarez-Builla J, Cai JJ, Bazan NG. Transcriptomic signature, bioactivity and safety of a non-hepatotoxic analgesic generating AM404 in the midbrain PAG region. Sci Rep. 2024;14:11103. https://doi.org/10.1038/s41598-024-61791-z.
28. Park K, Skidmore S, Hadar J, Garner J, Park H, Otte A, Soh BK, Yoon G, Yu D, Yun Y, Lee BK, Jiang X, Wang Y. Injectable, long-acting PLGA formulations: Analyzing PLGA and understanding microparticle formation. J Controlled Release. 2019;304:125–34. https://doi.org/10.1016/j.jconrel.2019.05.003.
29. Di Francesco M, Primavera R, Summa M, Pannuzzo M, Di Francesco V, Di Mascolo D, Bertorelli R, Decuzzi P. Engineering shape-defined PLGA microPlates for the sustained release of anti-inflammatory molecules. J Controlled Release. 2020;319:201–12. https://doi.org/10.1016/j.jconrel.2019.12.039.
30. Murgia D, Estevão BM, Portioli C, Palomba R, Decuzzi P. Optimizing the Fabrication of Shape-Defined Microparticles for Sustained Drug Delivery: The Less Is More Paradigm. ACS Appl Eng Mater. 2024;2:2535–48. https://doi.org/10.1021/acsaenm.4c00423.
31. Mayer JB, Patil SM, Shin S-H, Yoo J, Won Y-Y, Acceleration IW-I. Chemical Pathways, and Contributing Factors in the Degradation of Poly(lactic-co-glycolic acid) (PLGA) Microparticles and

Devices, ACS Biomater. Sci Eng. 2025;11:3932–48. https://doi.org/10.1021/acsbiomaterials.5c00419.

32. Bruschi ML. Mathematical models of drug release, in: Strateg. Modify Drug Release Pharm. Syst., Elsevier, 2015: pp. 63–86. https://doi.org/10.1016/B978-0-08-100092-2.00005-9
33. Trucillo P. Drug Carriers: A Review on the Most Used Mathematical Models for Drug Release. Processes. 2022;10:1094. https://doi.org/10.3390/pr10061094.
34. An J, Chen B, Kang X, Zhang R, Guo Y, Zhao J, Yang H. Neuroprotective effects of natural compounds on LPS-induced inflammatory responses in microglia. Am J Transl Res. 2020;12:2353–78.
35. Yu T, Li Z, Jia Z, Clapcote SJ, Liu C, Li S, Asrar S, Pao A, Chen R, Fan N, Carattini-Rivera S, Bechard AR, Spring S, Henkelman RM, Stoica G, Matsui S-I, Nowak NJ, Roder JC, Chen C, Bradley A, Yu YE. A mouse model of Down syndrome trisomic for all human chromosome 21 syntenic regions. Hum Mol Genet. 2010;19:2780–91. https://doi.org/10.1093/hmg/ddq179.
36. Rueda N, Flórez J, Martínez-Cué C. Mouse Models of Down Syndrome as a Tool to Unravel the Causes of Mental Disabilities, Neural Plast. 2012 (2012) 1–26. https://doi.org/10.1155/2012/584071
37. Scherma M, Justinová Z, Zanettini C, Panlilio LV, Mascia P, Fadda P, Fratta W, Makriyannis A, Vadivel SK, Gamaleddin I, Le Foll B, Goldberg SR. The anandamide transport inhibitor AM404 reduces the rewarding effects of nicotine and nicotine-induced dopamine elevations in the nucleus accumbens shell in rats. Br J Pharmacol. 2012;165:2539–48. https://doi.org/10.1111/j.1476-5381.2011.01467.x.
38. Mohar I, Stamper BD, Rademacher PM, White CC, Nelson SD, Kavanagh TJ. Acetaminophen-induced liver damage in mice is associated with gender-specific adduction of peroxiredoxin-6. Redox Biol. 2014;2:377–87. https://doi.org/10.1016/j.redox.2014.01.008.
39. Gonçalves AC, Coelho AM, Da Cruz Castro ML, Pereira RR, Da Silva Araújo NP, Ferreira FM, Machado Júnior PA, Pio S, Vital CE, Bezerra FS, Talvani A, De Castro Borges W, De Oliveira EC, Costa DC. Modulation of Paracetamol-Induced Hepatotoxicity by Acute and Chronic Ethanol Consumption in Mice: A Study Pilot. Toxics. 2024;12:857. https://doi.org/10.3390/toxics12120857.
40. Högestätt ED, Jönsson BAG, Ermund A, Andersson DA, Björk H, Alexander JP, Cravatt BF, Basbaum AI, Zygmunt PM. Conversion of Acetaminophen to the Bioactive N-Acylphenolamine AM404 via Fatty Acid Amide Hydrolase-dependent Arachidonic Acid Conjugation in the Nervous System. J Biol Chem. 2005;280:31405–12. https://doi.org/10.1074/jbc.M501489200.
41. Huang H-J, Chen S-L, Huang H-Y, Sun Y-C, Lee G-C, Lee-Chen G-J, Hsieh-Li HM, Su M-T. Chronic low dose of AM404 ameliorates the cognitive impairment and pathological features in hyperglycemic 3xTg-AD mice. Psychopharmacology. 2019;236:763–73. https://doi.org/10.1007/s00213-018-5108-0.
42. Zani A, Braida D, Capurro V, Sala M. Delta9-tetrahydrocannabinol (THC) and AM 404 protect against cerebral ischaemia in gerbils through a mechanism involving cannabinoid and opioid receptors. Br J

Pharmacol. 2007;152:1301–11. https://doi.org/10.1038/sj.bjp.0707514.

43. Bitencourt RM, Pamplona FA, Takahashi RN. Facilitation of contextual fear memory extinction and anti-anxiogenic effects of AM404 and cannabidiol in conditioned rats. Eur Neuropsychopharmacol. 2008;18:849–59. https://doi.org/10.1016/j.euroneuro.2008.07.001.
44. Adamczyk P, Gołda A, McCreary AC, Filip M, Przegaliński E. Activation of endocannabinoid transmission induces antidepressant-like effects in rats. J Physiol Pharmacol Off J Pol Physiol Soc. 2008;59:217–28.
45. García-Arencibia M, González S, De Lago E, Ramos JA, Mechoulam R, Fernández-Ruiz J. Evaluation of the neuroprotective effect of cannabinoids in a rat model of Parkinson's disease: Importance of antioxidant and cannabinoid receptor-independent properties. Brain Res. 2007;1134:162–70. https://doi.org/10.1016/j.brainres.2006.11.063.
46. Abush H, Akirav I. Cannabinoids modulate hippocampal memory and plasticity. Hippocampus. 2010;20:1126–38. https://doi.org/10.1002/hipo.20711.
47. Bellotti E, Contarini G, Geraci F, Torrisi SA, Piazza C, Drago F, Leggio GM, Papaleo F, Decuzzi P. Long-lasting rescue of schizophrenia-relevant cognitive impairments via risperidone-loaded microPlates. Drug Deliv Transl Res. 2022;12:1829–42. https://doi.org/10.1007/s13346-021-01099-x.
48. Saliba SW, Bonifacino T, Serchov T, Bonanno G, de Oliveira ACP, Fiebich BL. Neuroprotective Effect of AM404 Against NMDA-Induced Hippocampal Excitotoxicity. Front Cell Neurosci. 2019;13:566. https://doi.org/10.3389/fncel.2019.00566.
49. Coomey R, Stowell R, Majewska A, Tropea D. The Role of Microglia in Neurodevelopmental Disorders and their Therapeutics. Curr Top Med Chem. 2020;20:272–6. https://doi.org/10.2174/1568026620666200221172619.
50. Wilcock DM, Griffin WST. Down's syndrome, neuroinflammation, and Alzheimer neuropathogenesis. J Neuroinflammation. 2013;10:84. https://doi.org/10.1186/1742-2094-10-84.
51. Costa B, Siniscalco D, Trovato AE, Comelli F, Sotgiu ML, Colleoni M, Maione S, Rossi F, Giagnoni G. AM404, an inhibitor of anandamide uptake, prevents pain behaviour and modulates cytokine and apoptotic pathways in a rat model of neuropathic pain. Br J Pharmacol. 2006;148:1022–32. https://doi.org/10.1038/sj.bjp.0706798.
52. The Jackson Laboratory. Body Weight Information for B6 (000664) JAX® Mice Strain C57BL/6J, (n.d.). https://www.jax.org/jax-mice-and-services/strain-data-sheet-pages/body-weight-chart-000664
53. Di Francesco M, Bedingfield SK, Di Francesco V, Colazo JM, Yu F, Ceseracciu L, Bellotti E, Di Mascolo D, Ferreira M, Himmel LE, Duvall C, Decuzzi P. Shape-Defined microPlates for the Sustained Intra-articular Release of Dexamethasone in the Management of Overload-Induced Osteoarthritis. ACS Appl Mater Interfaces. 2021;13:31379–92. https://doi.org/10.1021/acsami.1c02082.
54. Bedingfield SK, Colazo JM, Di Francesco M, Yu F, Liu DD, Di Francesco V, Himmel LE, Gupta MK, Cho H, Hasty KA, Decuzzi P, Duvall CL. Top-Down Fabricated microPlates for Prolonged, Intra-articular

Matrix Metalloproteinase 13 siRNA Nanocarrier Delivery to Reduce Post-traumatic Osteoarthritis. ACS Nano. 2021;15:14475–91. https://doi.org/10.1021/acsnano.1c04005.

55. Primavera R, Bellotti E, Di Mascolo D, Di Francesco M, Wang J, Kevadiya BD, De Pascale A, Thakor AS, Decuzzi P. Insulin Granule-Loaded MicroPlates for Modulating Blood Glucose Levels in Type-1 Diabetes. ACS Appl Mater Interfaces. 2021;13:53618–29. https://doi.org/10.1021/acsami.1c16768.
56. Saura J, Tusell JM, Serratosa J. High-yield isolation of murine microglia by mild trypsinization. Glia. 2003;44:183–9. https://doi.org/10.1002/glia.10274.
57. ISO 10993-5. :2009, Biological Evaluation of Medical Devices—Part 5: Tests for in Vitro Cytotoxicity., (2009). https://www.iso.org/standard/36406.html
58. Deidda G, Parrini M, Naskar S, Bozarth IF, Contestabile A, Cancedda L. Reversing excitatory GABAAR signaling restores synaptic plasticity and memory in a mouse model of Down syndrome. Nat Med. 2015;21:318–26. https://doi.org/10.1038/nm.3827.

Figures

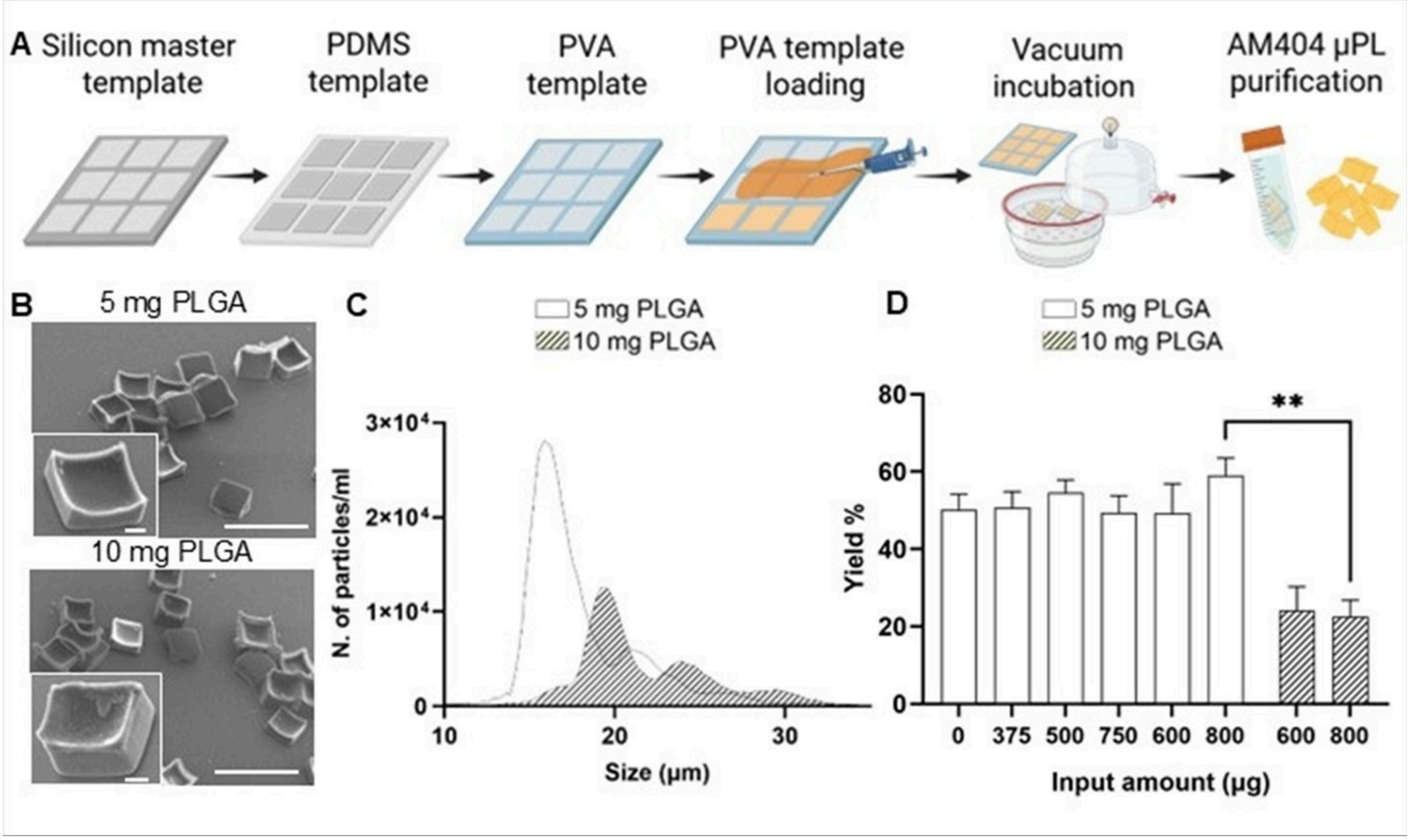


Figure 1

A top-down fabrication method for µPL with varying polymer and AM404 inputs. A. Sequential steps in the top-down fabrication process of 20 µm (edge length) by 10 µm (height) square-based µPL. **B.**Representative scanning electron micrographs of 5 mg PLGA and 10 mg PLGA µPL (scale bar = 50

μm). Insets present μPL at higher magnification (scale bar = 5 μm). **C**. Representative Multisizer Coulter counter profiles for 5 mg and 10 mg μPL. **D.** Fabrication yield for all tested configurations. Bars represent the average of at least three different replicates ± SEM. One-way ANOVA followed by Šídák's multiple comparisons test: ** p = 0.0055 – 10 mg PLGA μPL with 800 μg vs. 5 mg PLGA 800 μg.

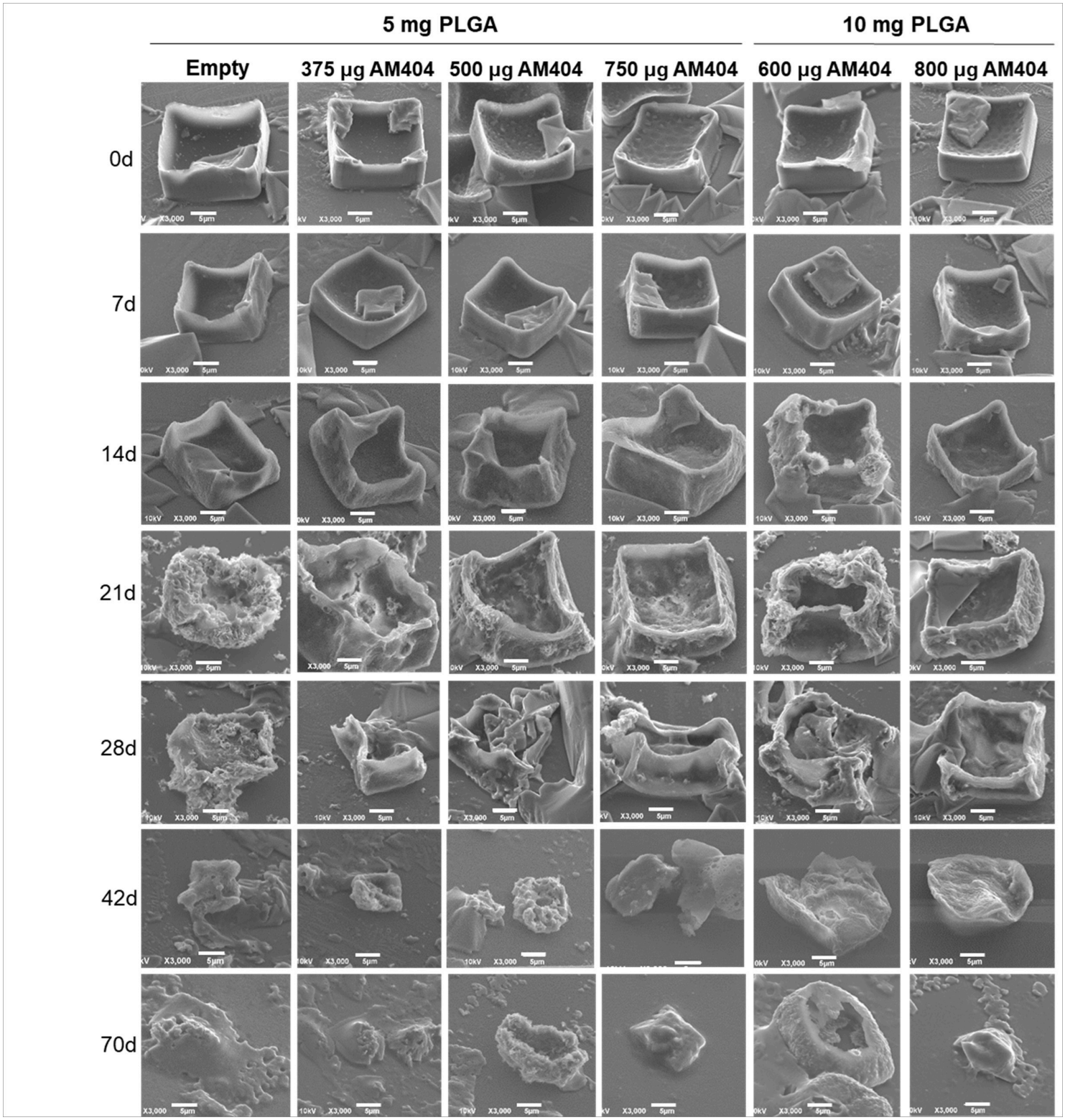


Figure 2

Biodegradation of µPL. Representative high magnification (×3,000) scanning electron microscopy images of µPL in PBS at different time points up to 70 days (d). Different µPL configurations are considered: empty or loaded with different amounts of AM404, namely 5 mg of PLGA with 375 µg, 500 µg, or 750 µg AM404; and 10 mg of PLGA with 600 µg or 800 µg AM404) (Scale bars = 5 µm).

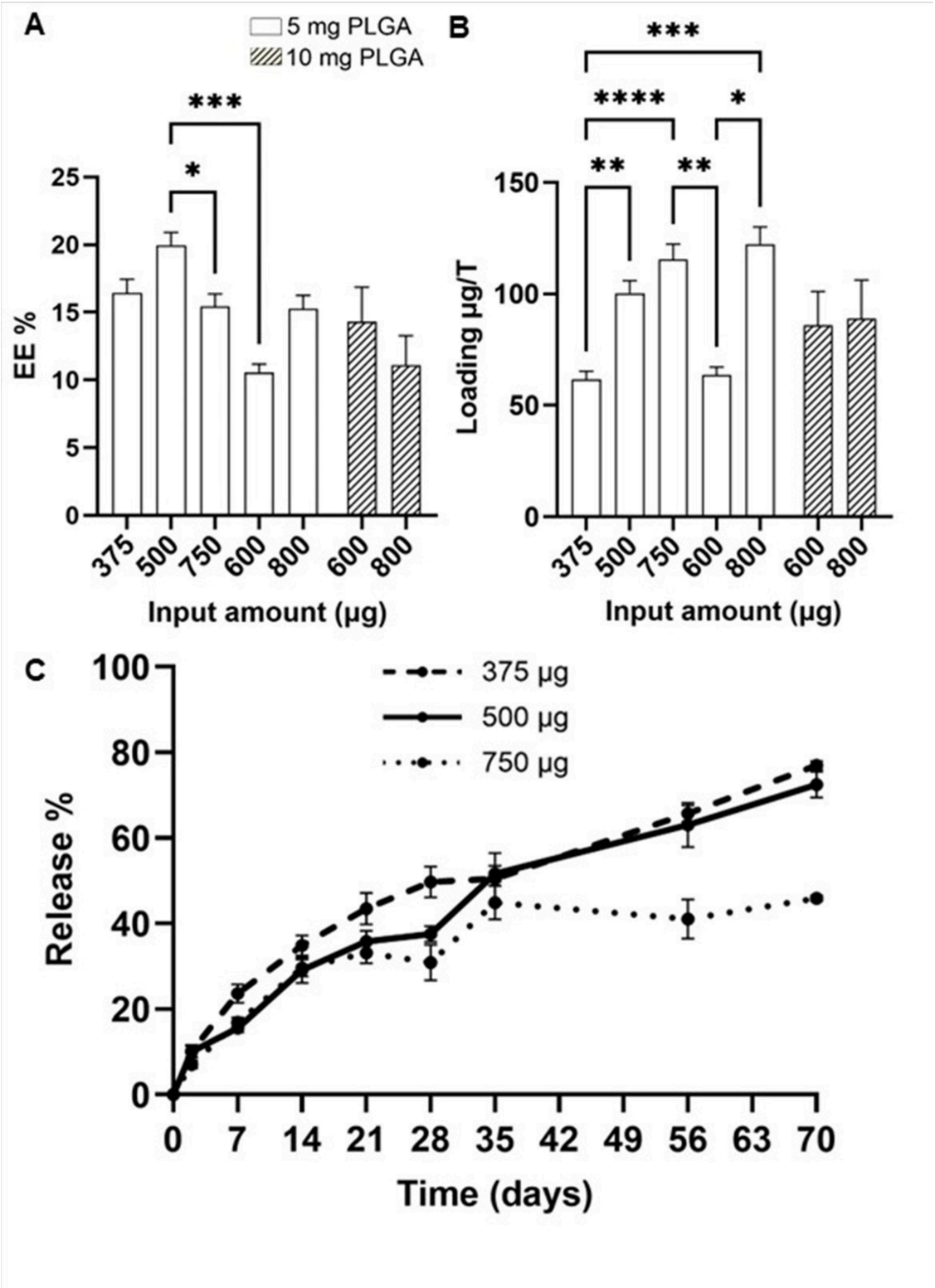


Figure 3

Pharmacological characterization of AM404–μPL. A. Encapsulation efficiency (EE) of AM404 for different input amounts, namely 375 μg, 500 μg, 600 μg, 750 μg, or 800 μg of AM404 in the 5 mg PLGA μPL (white bars) and 600 μg or 800 μg of AM404 in the 10 mg PLGA μPL (hatched bars). One-way ANOVA followed by Šídák's multiple comparisons test: *** p= 0.0007 – 500 μg 5 mg PLGA vs. 600 μg 5 mg PLGA, * p= 0.0169 – 500 μg 5 mg PLGA vs. 750 μg 5 mg PLGA. **B**. Loading of AM404 per PVA template for different input amounts, namely 375 μg, 500 μg, 600 μg, 750 μg, or 800 μg of AM404 in the 5 mg PLGA μPL (white bars) and 600 μg or 800 μg of AM404 in the 10 mg PLGA μPL (hatched bars). One-way ANOVA followed by Šídák's multiple comparisons test: **** p<0.0001 – 375 μg 5 mg PLGA vs. 750 μg 5 mg PLGA, *** p=0.0009 – 375 μg 5 mg PLGA vs. 800 μg 5 mg PLGA, ** p=0.0049 – 375 μg 5 mg PLGA vs. 500 μg 5 mg PLGA, ** p=0.0037 – 750 μg 5 mg PLGA vs. 600 μg 5 mg PLGA, * p=0.0144 – 600 μg 5 mg PLGA vs. 800 μg 5 mg PLGA. **C**. Release study of AM404 from different 5 mg μPL configurations in PBS. The release was monitored for up to 70 days and is represented by the percentage of AM404 released compared to the initial loaded amount at time 0 over time (days). Bars represent the average of at least three different replicates ± SEM.

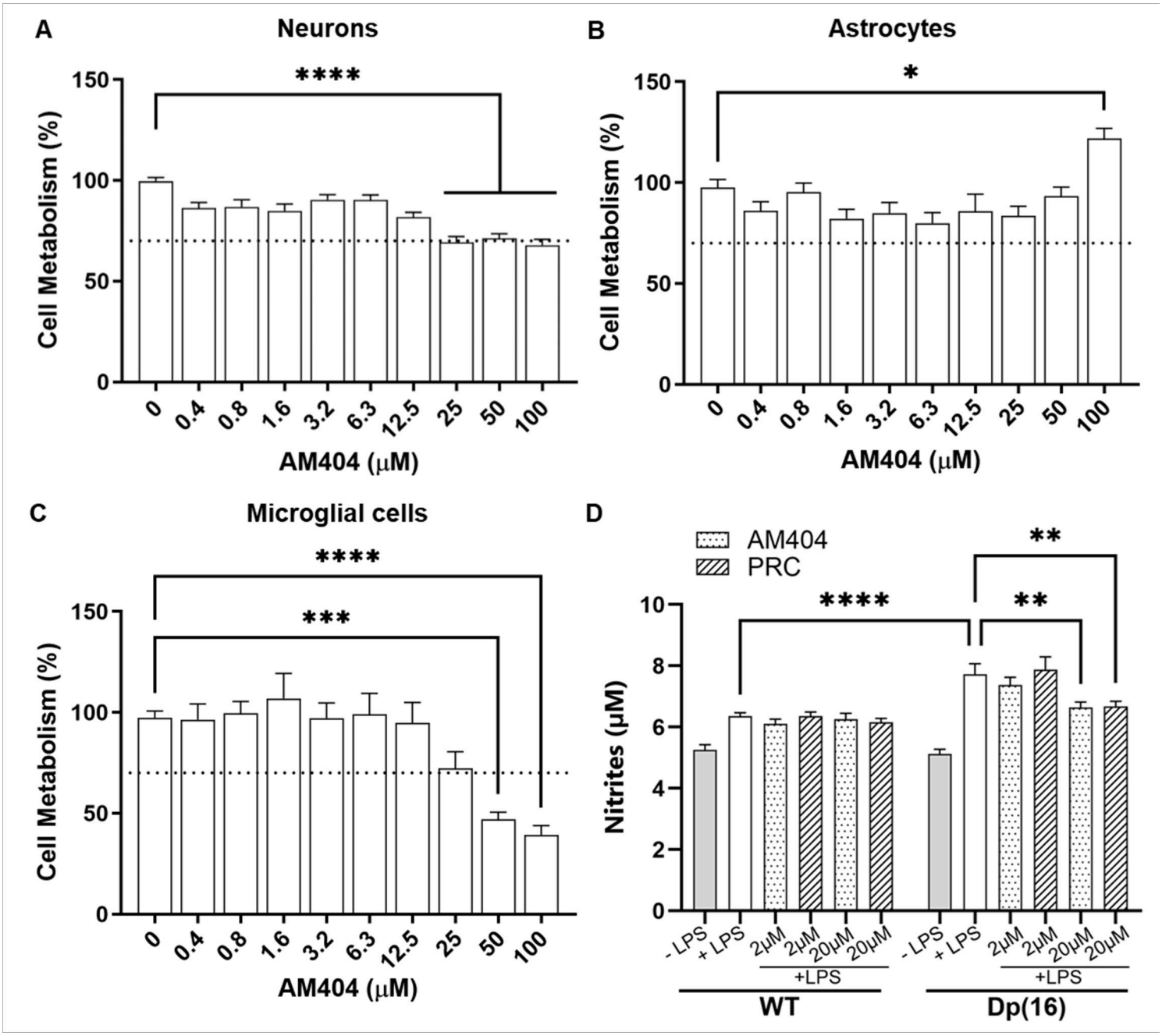


Figure 4

Cytotoxicity and therapeutic efficacy of free AM404. MTT assay on primary cell cultures of neurons (**A**), astrocytes (**B**), and microglial cells (**C**) treated with increasing concentrations of AM404 up to 100 μM. The dotted line in the plots indicates the cell metabolism interference at 70% cell viability relative to the control. A decrease in cell viability exceeding 30% is classified as cytotoxic. Bars represent the mean ± SEM. One-way ANOVA followed by Šídák's multiple comparisons test determined statistical significance, with ****p<0.0001 – 0 μM (neurons) vs. 12.5 μM (neurons), 25 μM (neurons), 50 μM (neurons), 100 μM (neurons), **p = 0.0071 – 0 μM (neurons) vs. 0.4 μM (neurons), **p = 0.0012 – 0 μM (neurons) vs. 1.6 μM (neurons), *p = 0.0306 – 0 μM (neurons) vs. 0.8 μM (neurons), *p=0.0193 – 0 μM (astrocytes) vs. 100 μM (astrocytes), ***p = 0.0002 – 0 μM (microglia) vs. 50 μM (microglia), ****p<0.0001 – 0 μM (microglia) vs. 100 μM (microglia). **D**. Griess assay to quantify the production of nitrites from cultures of primary

microglial cells derived from wild type (WT) and Dp(16) littermates, treated with 2 μM or 20 μM of free AM404 or paracetamol (PRC) and inflamed with 100 ng/mL LPS. Bars represent the mean ± SEM. One-way ANOVA followed by Šídák's multiple comparisons test determined statistical significance, with ****p<0.0001 – control WT vs. control Dp(16), **p=0.0092 – control Dp(16) vs. PRC 20 μM Dp(16), **p=0.0059 – control Dp(16) vs. AM404 20 μM Dp(16).

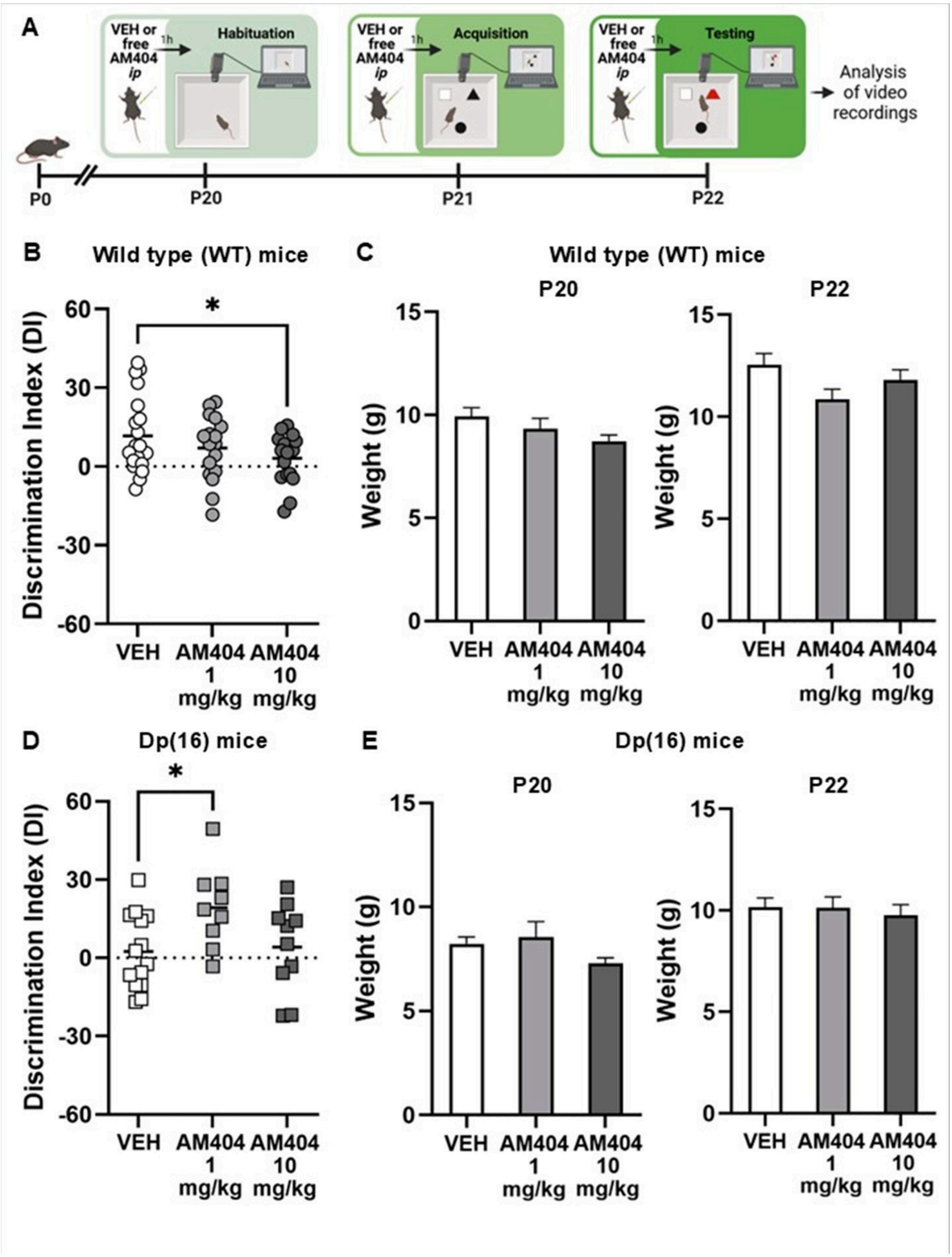


Figure 5

Improved cognitive functions of Dp(16) mice treated with low dose AM404. A. Schematic representation of the experimental protocol involving the injection of vehicle (VEH) or free AM404 (1 mg/kg or 10 mg/kg) in WT and Dp(16) on postnatal days P20 (day 1), P21 (day 2), and P22 (day 3). On days P20 to P22, we conducted the Novel Object Recognition (NOR) behavioral test, which included the Habituation, Acquisition, and Testing phases. **B.** Representation of the Discrimination Index (DI) obtained from NOR tests performed at P22 by WT mice upon VEH or AM404 treatments (AM404 1 mg/kg or AM404 10 mg/kg). Bars illustrate the average DI of all analyzed mice ± SEM, and symbols denote individual data points for each animal (**p*=0.0477, Unpaired t-test). **C.** Weights of WT mice were assessed at P20 (beginning of treatment) and P22 (end of treatment) to evaluate potential toxic effects of VEH or AM404 treatments. Bars show the mean ± SEM. **D.** Representation of DI obtained from NOR tests performed at P22 by Dp(16) mice upon VEH or AM404 treatments. Bars indicate the average DI of all analyzed mice, and symbols represent individual data points for each animal (**p*=0.0149 – Unpaired t-test). **E**. Weights of Dp(16) mice assessed at P20 (beginning of the treatment) and P22 (end of treatment) to evaluate potential toxic effects of VEH or AM404 treatments. Bars depict the mean ± SEM.

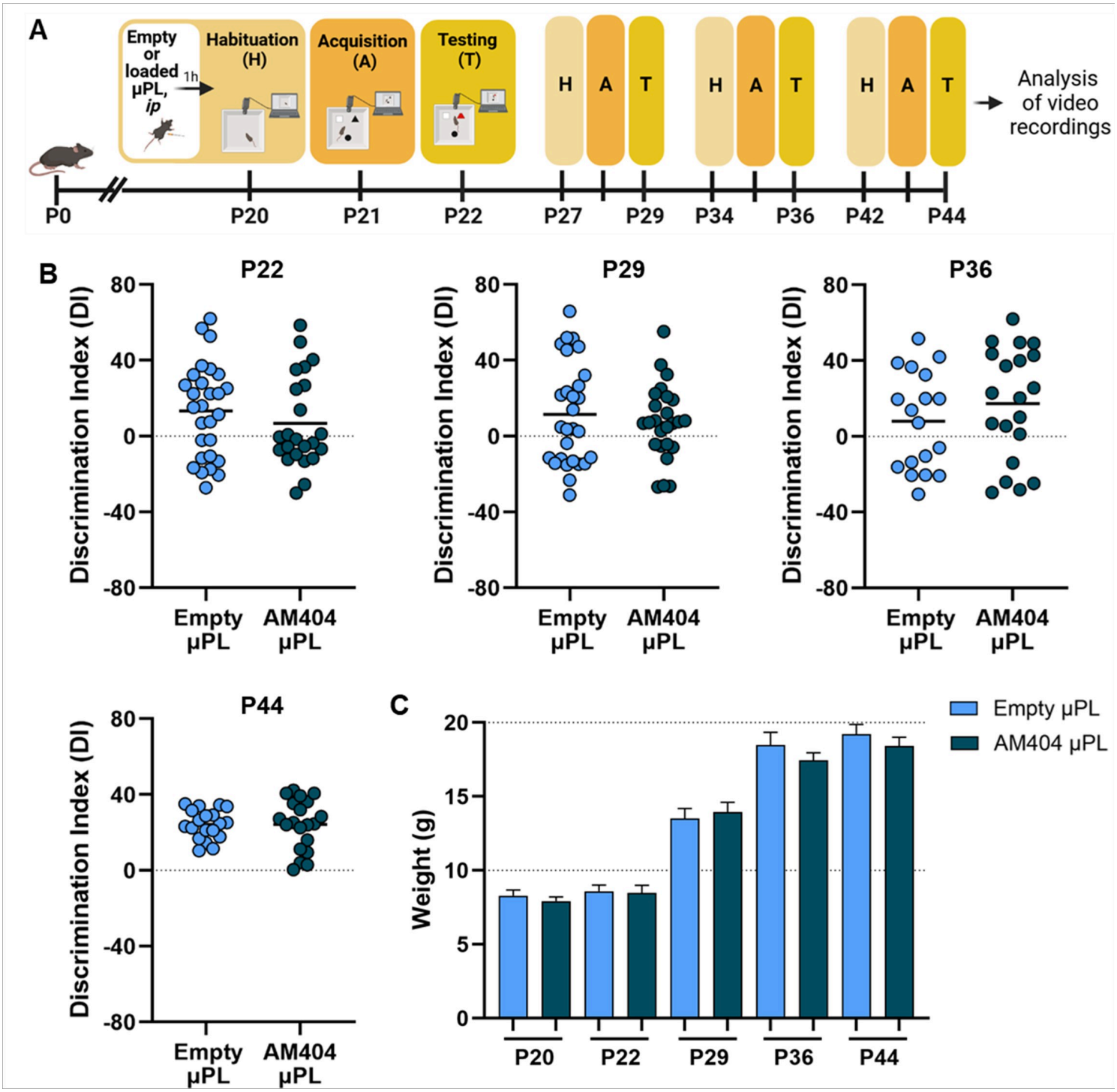


Figure 6

Cognitive function of WT mice treated with empty µPL and AM404–µPL. A. Schematic representation of the experimental protocol involving a single injection of µPL loaded with AM404 and an empty µPL as a control. Mice were injected at P20, and the NOR test was performed at P22, P29, P36, and P44, with Habituation (H) on day 1, Acquisition (A) on day 2, and Testing (T) on day 3. **B**. Representation of the discrimination index (DI) obtained from NOR tests performed at P22, P29, P36, and P44, by WT mice upon empty µPL or AM404–µPL treatments. Bars represent the average DI of all analyzed mice ± SEM, while the symbols indicate individual data points for each animal. **C**. Weights of WT mice were assessed

at P20 (beginning of the treatment), and P22, P29, P36, and P44, to evaluate potential toxic effects of empty or AM404–µPL treatments. Bars display the mean ± SEM.

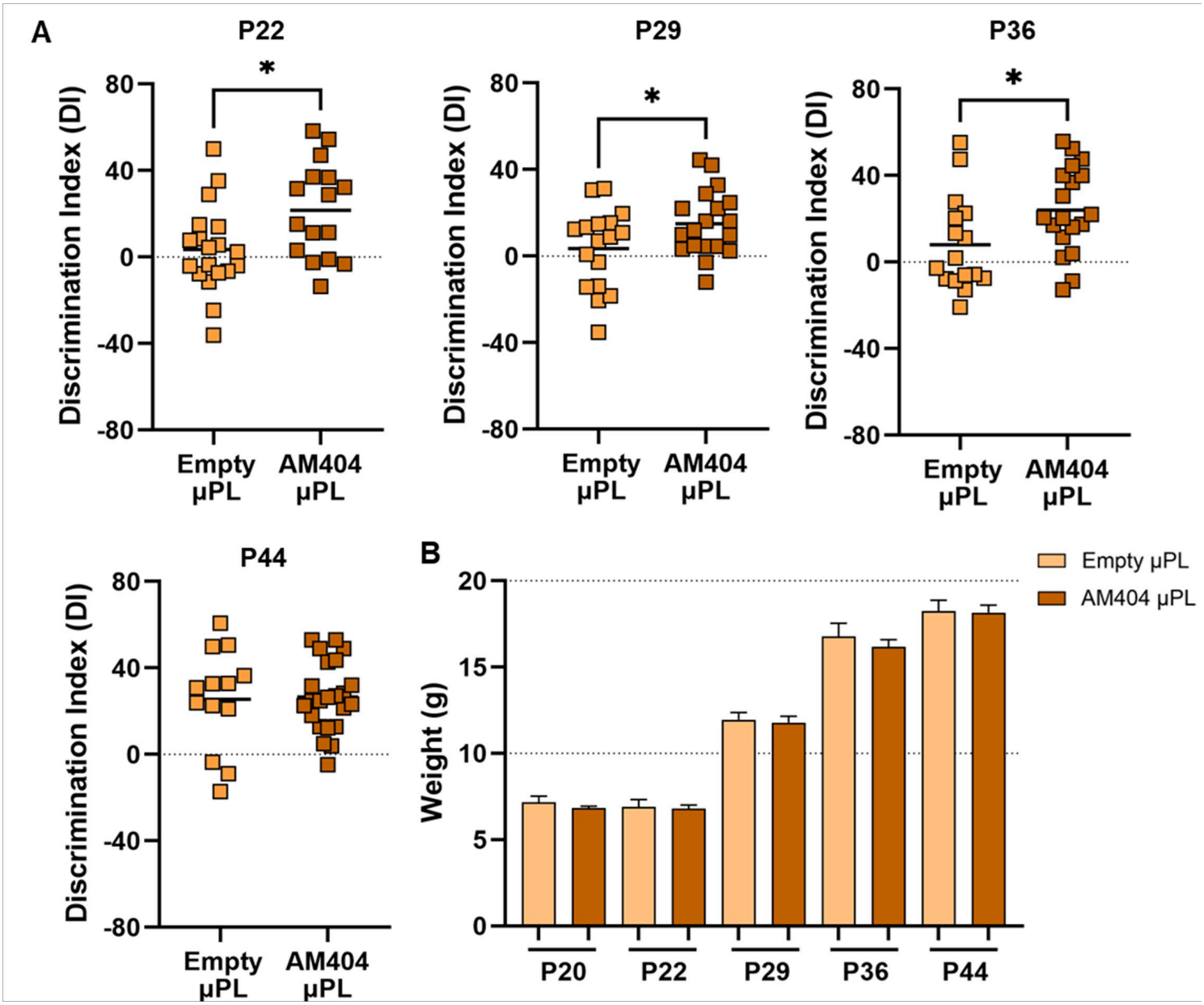


Figure 7

Extended improved cognitive functions of Dp(16) mice treated with one dose of AM404–µPL. A. Representation of the discrimination index (DI) obtained from NOR tests performed at P22, P29, P36, and P44, by Dp(16) mice upon empty µPL or AM404–µPL treatments. Bars indicate the average DI of all analyzed mice ± SEM, while symbols represent individual data points for each animal (Unpaired t-test: at P22 *p=0.0145, at P29 *p=0.0347, at P36 *p=0.0487). **B**. Weight of Dp(16) mice assessed at P20 (beginning of the treatment), and P22, P29, P36, and P44, to evaluate potential toxic effects of empty or AM404–µPL treatments. Bars show the mean ± SEM.

Supplementary Files

This is a list of supplementary files associated with this preprint. Click to download.

- AM404uPLSupportingInformation5July26.docx